UCRL 9362

UNIVERSITY OF CALIFORNIA

Ernest O. Lawrence

Radiation Laboratory

DIFFERENTIAL ELASTIC PION - PROTON SCATTERING AT 600, 650, AND 750 Mev

DISCLAIMER

cy 2

UC-34 Physics and Mathematics

University of California
Lawrence Radiation Laboratory
Berkeley, California

January 27, 1961

TO: Recipients of UCRL-9362

FROM: Technical Information Division

SUBJECT: ERRATA, UCRL-9362, Differential Elastic Pion-Proton Scattering at 600, 650, and 750 Mev (Thesis), John I. Shonle, August 12, 1960.

P. 4, l. 13: Delete first two words, "in 1958".

P. 6, l. 3 from bottom: Change "Wong and Ross, and Peierls" to "Wong and Ross, [31] and Peierls".

P. 7, l. 1: Delete superscript "31".

P. 7, l. 11: Change " ... a pion-pion entrance channel. " to "... a pion-pion entrance channel. [33]".

P. 7, l. 13: Delete superscript "33".

P. 7, l. 5-4 from bottom: Change "Statistical operations were also improved ..." to "The number of events was also increased ...".

P. 11, l. 2 from bottom: Change "After a scan card made ..." to "After a scan card was made ...".

P. 15, l. 8 from bottom: Change "investigations of identifying-events and ..." to "investigations for identifying events and ...".

P. 17, l. 7: Change "and to knock it out so that the " to "and can knock it out so that the".

P. 22, l. 8 from bottom and bottom line: Change "$X_{\frac{\Delta c}{c} r}$ " to "$x_{\frac{\Delta c}{c} r}$ ".

P. 29, l. 4: Change "$X_{\frac{\Delta c}{c} r}$ " to "$x_{\frac{\Delta c}{c} r}$ ".

P. 29, l. 4: Change "1/4-σ" to "(1/4)σ".

P. 31, l. 5: Change "...sum of the squares of the deviations, from the average..." to "sum of the squares of the deviations from the average,".

P. 32, l. 3: Change "The data are divided by the scanning efficiency." to "The data are divided by the scanning efficiency as given below."

P. 42, l. 10-11: Change " ...which left the chamber as a stopping proton." to " ...which left the chamber a stopping proton."

P. 45, l. 6: Change "every tenth picture, was counted..." to "every tenth picture was counted..."

P. 47, l. 7 from bottom: Change "H-magnet and the collimator, which remained..." to "H-magnet and the collimator which remained...".

P. 48, l. 20: Change "of the electrons will lose the state amount..." to "of the electrons will lose the stated amount...".

P. 50, Fig. 10: Blacken the circle at 770 Mev.

P. 52: Substitute new p. 52, with corrected Fig. 11.

P. 53, bottom line: Change "This criterion selects third, fourth, and fifth degrees." to "This criterion selects fourth, fourth, and fifth degrees."

P. 55, l. 14" Change "The lowest contribution to $(\cos \theta^*)$ comes ..." to "The lowest contribution to $(\cos \theta^*)^5$ comes ...".

P. 55, l. 15: Delete superscript "5".

P. 57, footnote[a] should read: $\frac{d\sigma}{d\Omega} = \sum_n a_n (\cos \theta^*)^n$, in mb/sr.

P. 59: The two-line formula should read:

$$\text{"}\frac{d\sigma}{d\Omega} = \ldots P_\ell (\cos \theta^*) \ldots P_\ell (\cos \theta^*) \ldots$$

P. 60: Substitute new p. 60, with corrected Fig. 14.

P. 63, l. 13: Change"...must increase and n must " to "...must increase and then".

P. 63, l. 11: Change "it resonance or non-resonance" to "its resonance or nonresonance."

P. 67, l. 9: Change "All of the measures who meas-" to "All of the measurers who meas-".

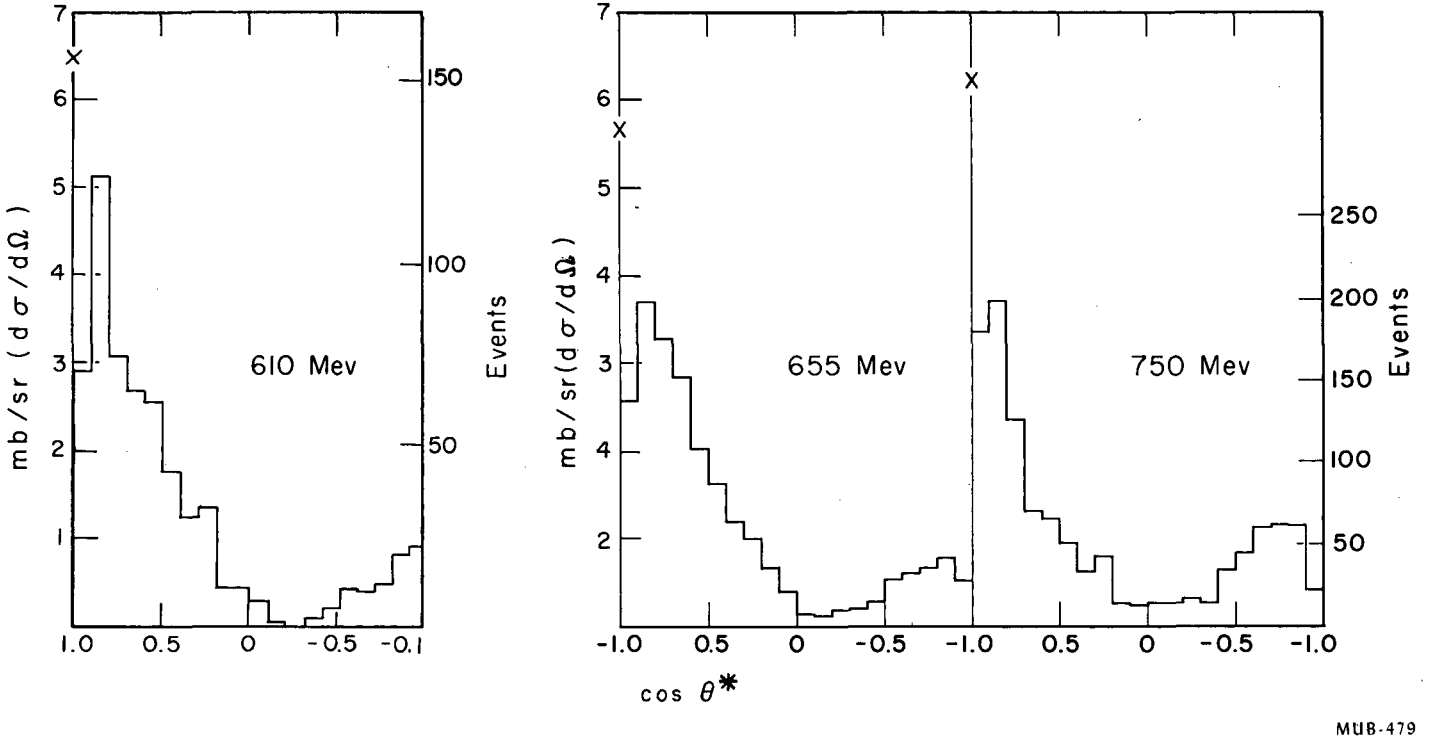

Fig. 11. Differential elastic cross sections at 610, 655, and 750 Mev. The numbers of events in each interval of cosine are indicated on right-hand scales. The forwardmost interval is not corrected for the small-angle bias. Crosses indicate the forward scattering calculated from the optical theorem and dispersion relations (see Sec. VI).

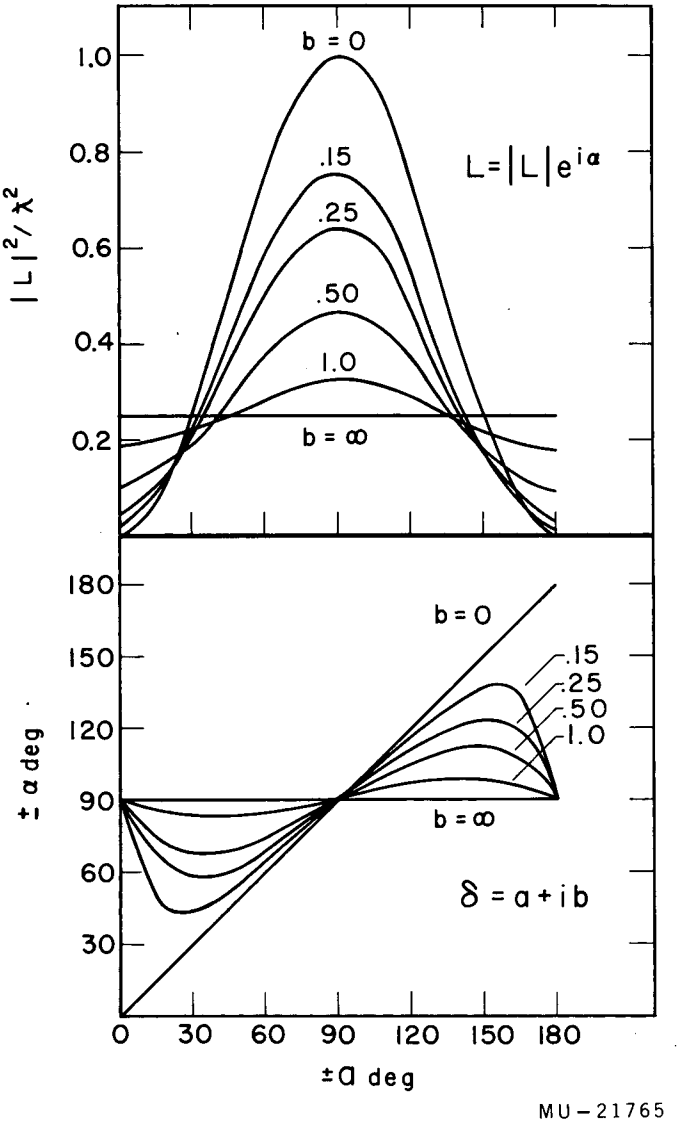

Fig. 14. Variation of the magnitude and phase of the scattering amplitude, as defined in Sec. VI, with the real and imaginary parts of the phase shift, where $L = |L| e^{i\alpha}$, and $\delta = a + ib$.

Research and Development - Thesis

UCRL-9362
UC-34 Physics and
Mathematics
TID-4500 (15 th Ed.)

UNIVERSITY OF CALIFORNIA
Lawrence Radiation Laboratory
Berkeley, California

Contract No. W-7405-eng-48

DIFFERENTIAL ELASTIC PION – PROTON SCATTERING AT 600, 650, AND 750 MEV

John I. Shonle
(Thesis)

August 12, 1960

Printed in USA. Price $1.75. Available from the
Office of Technical Services
U. S. Department of Commerce
Washington 25, D.C.

DIFFERENTIAL ELASTIC PION – PROTON SCATTERING AT 600, 650, AND 750 MEV

Contents

DIFFERENTIAL ELASTIC PION – PROTON SCATTERING AT 600, 650, AND 750 MEV

John I. Shonle
(Thesis)

Lawrence Radiation Laboratory
University of California
Berkeley, California

August 12, 1960

ABSTRACT

The differential elastic cross sections for π^--p scattering have been measured at 610 ± 20, 655 ± 20, and 750 ± 20 Mev in a propane bubble chamber. The elastic events were selected by a χ^2 test. The total elastic cross sections are 17.7 ± 2.3, 16.6 ± 1.4, and 14.8 ± 1.4 mb, respectively. Cosine-power series were fitted to the angular distributions. The variation of the coefficients with energy indicates $J = 3/2$ for the 600-Mev resonance and $J = 5/2$ for the 890-Mev resonance in the π^--p interaction. The data were more compatible with odd relative parity for the two: $P_{3/2}$ and $D_{5/2}$, or $D_{3/2}$ and $F_{5/2}$. Thus the scattering data independently give the same assignments for the peaks as the photo-production data. Resonance at the peaks is not established, but is the most plausible explanation for them. Strong absorption of the $J = 3/2$ resonant wave is suggested.

I. INTRODUCTION

The early measurements of the π^--proton total cross section by Cool, Piccioni, and Clark showed a broad maximum at about 0.9-Bev laboratory kinetic energy.[1] Subsequent measurements of the photo-production of π^+ [2-4] and π^0 [5-9] mesons from hydrogen showed a relatively sharp peak at a photon energy of 750 Mev. This peaking was especially evident in the energy dependence of the π^+ production at 90 deg (center-of-momentum system).[3] Location and width of the photo-production peak did not correspond to that in the π^--proton scattering cross section. The maximum found by Cool et al. would be expected to show up at a photon energy of about 1.0 Bev. However, work at the California Institute of Technology indicated that there was another closely spaced peak at a somewhat higher energy.[4] Wilson suggested in 1958 that there were two closely spaced peaks which had not been separately resolved by Cool et al., the lower of which was found at 750-Mev photon energy.[10] The photo-production cross section at 90 deg (c.m.s.) for π^+ was about twice that of the π^0, indicating that the peak was predominantly due to an isospin-1/2 state. Burrowes et al., running with a well-defined beam and measuring at closely spaced energy intervals, were able to resolve two separate peaks in the π^--p total scattering cross section.[11] They also took data on the π^+-p total cross section for the same energy region. This cross section varied smoothly with energy, showing no trace of the maxima. Since the π^+-p system is in a pure isospin state of 3/2, while the π^--p system is a mixture of 3/2 and 1/2, this cross section measurement verified that the peaks were due to an interaction in the isospin-1/2 state. The energy of the lower of these two peaks did not agree with the corresponding photon energy for the photo-production peak, but the absolute energy calibration of Burrowes et al. was not reliable. Subsequent experiments at Berkeley[12] and Saclay[13] were in agreement with each other and the photo-production data, fixing the energy of the lower peak at 600 ± 10 Mev and the higher at 890 ± 10 Mev.

Previous π^--p elastic scattering experiments in this energy region have been made at 425,[14] 460,[15] 600,[15] 610,[16] 770,[15] 810,[17]

915,[18] 925,[19] 950,[20] 960 Mev,[21] and 1.0 Bev,[22] laboratory kinetic energies. The energy dependence of the total elastic cross section in general follows that of the total cross section.[15] The shapes of the differential elastic cross sections all show a strong forward peaking, and a smaller backwards hump which increases with energy and then decreases. It is hard to get good quantitative information from these differential cross section measurements because of the large energy spread and relatively low statistics of many of these experiments. Also one is reluctant to make too detailed a comparison of data gathered in different ways, due to uncertainties in biases and systematic errors which may vary from one experiment to the next.

These higher energy peaks in the pion cross sections are generally referred to as "resonances" although the resonant nature is not definitely established. Indeed the large π^+-p cross section, and the large forward peaking of the elastic scattering experiments, clearly shows that there is a large contribution of non-resonant states. However, it may be assumed that the peaks in the total cross section are due to a single state exhibiting a resonant behavior at each energy. Several orbital (L) and total angular momentum (J) assignments have been made to account for the peaks. Wilson gave a J value of 3/2 to the lower peak and suggested that it might be a P state and also that the next peak might have $J = 5/2$.[10] Peierls has assigned the lower peak to $D_{3/2}$ and the higher peak to $F_{5/2}$.[23,24] Bingham and Clegg gave a possible assignment of $P_{1/2}$ to the lower state.[8] Landovitz and Marshall show that $P_{3/2}$ and $D_{3/2}$ or $D_{5/2}$ are not inconsistent with the data.[25] All of the foregoing assignments have been based on photo-production data where the nonresonant states are not so strongly excited as in pion scattering. In particular, the π° angular distribution at the lower peak is approximately proportional to $(2 + 3 \sin^2 \theta^*)$, which implies $J = 3/2$.[24] However, the π° data are not so well-known as might be desired, and the π^+ data have the added confusion of the retardation term which has not always been properly taken into consideration in the foregoing analyses.[26,27] The polarization data of Stein show that states of odd relative parity are important at 550- and

700-Mev photon energies.[28] Sakurai suggested that the existence of the polarization was decisive for Peierls' assignment.[29] On the other hand, Landovitz and Marshall emphasize that it is not immediately evident which two states have the odd relative parity; that is, whether it is the $J = 3/2$, $T = 3/2$ and the lower of the $T = 1/2$ states, or the two $T = 1/2$ states which are relatively odd, where T is the total isospin. The energy dependence of the polarization found by Stein is more readily interpreted by the assignments of Landovitz and Marshall. But there are difficulties with their assignment with regard to the π^+ angular distribution around 500 Mev.

The elastic scattering experiments to date have been less suggestive as to the nature of the states responsible for the peaks. The diffraction-like forward peak indicates that there is strong absorption in several angular momentum states. Erwin and Kopp tried to analyze their data in the backward hemisphere in terms of P and D, or D and F, waves but were only able to conclude that no single state or pair of states really dominates.[20] A similar analysis in the backward direction by Feld et al. showed somewhat better consistency with $D_{3/2}$ -$F_{5/2}$ interference than with $P_{3/2}$ -$F_{5/2}$, although their analysis was based on the wrong values of the energies of the peaks, and other combinations were not tried and cannot be ruled out.[19]

Several theoretical explanations have been brought forth for these higher resonances. Wilson suggested the existence of new isobaric states of the nucleon, similar to the interpretation of the 190-Mev $J = 3/2$, $T = 3/2$ resonance as an isobar.[10] There is some evidence against this conjecture. Recent p-p inelastic scattering results showed evidence of the formation of the (3/2, 3/2) isobar but found no indication of the formation of isobars with masses corresponding to the peaks in the $T = 1/2$ state.[30] Peierls accounts for the lower peak in terms of a two-pion one-nucleon final state, in which one of the pions forms the (3/2, 3/2) isobar with the nucleon.[23] The other pion is in a relative S-wave state with respect to this isobar. Wong and Ross, and Peierls account for the higher $T = 1/2$ peak by assuming a series of vertices in a Feynman diagram, in which first one and then the other pion

scatters from the nucleon in the (3/2, 3/2) state.[31] Peierls uses a pion-nucleon core interaction with a pion-pion interaction as a non-resonant background to get a qualitative understanding of why apparently only $T = 1/2$ is important at these resonances. Carruthers has suggested that the $D_{3/2}$ resonance does occur in π^+-p scattering, but that it is displaced to a higher energy, is smaller, and is partially masked by another much broader resonance.[32] The work of Devlin et al. shows a shoulder at around 850 Mev which may be interpreted as such a resonance.[12] Carruthers and Bethe, extending all these ideas, suggest a model in which all of the resonant final-state interactions in either isospin state are initiated from a pion-pion entrance channel. They assume that the $T = 0$ state of the two pions is dominant around 600 Mev, and that the $T = 1$ state does not become important until above 800 Mev.[33] A $T = 0$ state of the pions can lead only to $T = 1/2$ for the pion-nucleon system as a whole. Thus the isospin and energy dependence of the higher resonances is governed by the pion-pion interaction and the (3/2, 3/2) resonance, according to these authors.

The present propane bubble-chamber experiment was undertaken to improve on the previous π^--p elastic scattering experiments, with the idea of bettering the understanding of these peaks. Sets of data at several closely-spaced energies were produced. Since the peaks in question are rather sharp, the energy spread was kept to that introduced by ionization of the particles traversing the chamber, which amounted to 40 Mev for the scanning region used. Statistical operations were also improved over some of the previous experiments. The energies selected (measured at the center of the chamber) were 610, 655, and 750 Mev, going from the maximum of the lower peak to the minimum between the two peaks where interference should be large.

II. EXPERIMENTAL DETAILS

This experiment was performed at the Bevatron using a 30-inch propane bubble chamber. The layout of the beam is shown in Fig. 1. Protons at an energy of 5.3 Bev struck an internal copper target placed in the west straight section. Pions were taken off at an angle of 30 deg (lab) from the beam direction and were passed out through a thin window in the vacuum tank. A steel pipe shielded the beam from the stray magnetic field of the Bevatron, but a small C-magnet was also placed to make fine compensations for any residual field. The beam then passed through two 4-inch diameter quadrupole triplets, the first essentially rendering the beam parallel, and the second bringing it to focus vertically at the chamber and horizontally at the momentum-defining collimator. The magnification of the system was close to unity in both directions. The beam was deflected 20° 5' by an H-magnet. Nineteen feet from the center of the H-magnet there was a lead-and-concrete collimator with an aperture 2 in. by 2 in. The part which actually defined the beam consisted of two castings of lead 12 inches apart, one 12 in. thick and the other 6 in. thick. The collimator was made in this manner to reduce slit scattering. The width of the collimator corresponds to a momentum spread of ± 1%. An additional ± 0.5% uncertainty comes from the finite target size. Immediately behind the collimator there was a single-section 4-inch quadrupole magnet (Q_3) to spread the beam horizontally to the width of the thin window of the chamber. A helium bag placed between Q_1 and the collimator reduced multiple scattering of the beam in air. Its introduction reduced the vertical spread of the beam from about 2 in. to about 1 in. Momenta of the beams were determined by the stretched current-carrying wire technique. Incoming momenta were also determined from the average measured curvature of beam tracks in the chamber. The wire-orbit values were also checked by comparing observed with expected proton ranges for elastic events (see Sec. III). All three methods were consistent within about 1%, which is the order of error. The wire-orbit values were used for the nominal momenta. Currents in the magnets were checked frequently during the run and had negligible drift. About

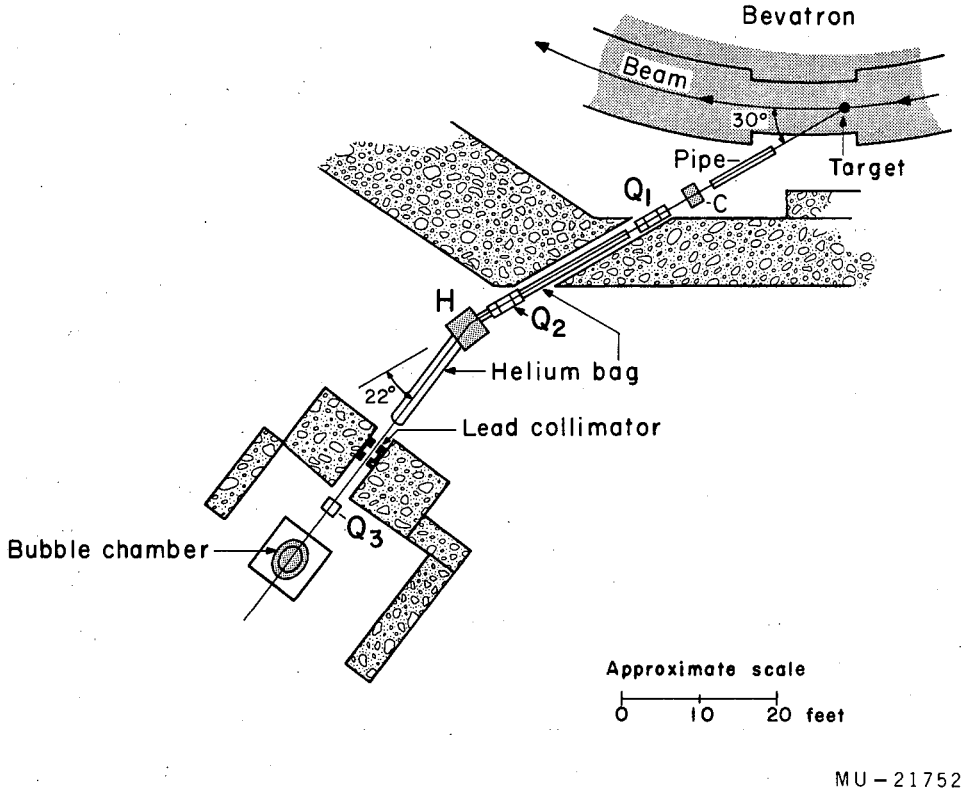

Fig. 1. Arrangement of the negative pion beam. Q_1, Q_2, and Q_3 are 4-inch quadrupole magnets. C is a compensating magnet, and H the momentum-defining magnet. The iron pipe shields from the stray magnetic field of the Bevatron.

15 to 20 pions per pulse entered the chamber, from about 2×10^9 protons on the target.

The chamber was so aligned that the beam was parallel to the edges of the support bars of the thin window at that point. The chamber, described in detail elsewhere,[34] operates with a 13-kG magnetic field. Principal changes in the chamber from earlier runs were the introduction of some sponge material around the edges of the propane container, and the running of the upper and lower heater systems at the same temperature to reduce the turbulence in the hydrostatic supporting oil. About 10,000 stereo-pairs of pictures were taken at each of the energies reported here.

The pictures were scanned using overhead projectors which could project either view separately or both superimposed, full size. The scanning region was defined as that region which, when projected to the bottom glass, was within ± 25 cm of the center of the chamber lengthwise. The full width of the chamber was used for scanning, but the beam was narrower than this width. Thus all events were located well away from the edges of the chamber except for the region near where the beam, having been bent by the magnetic field, left the chamber by a side wall. The beam was well-defined vertically, lying almost entirely within ± 1 in. of the median plane of the chamber (except as noted below). Thus most events occurred well away from the top or bottom, since the chamber is 6.5 in. deep. Unfortunately, at 610 Mev the beam was about 1 in. too low.

The scanners were carefully instructed to put down any two-pronged event which could possibly be a π^--p elastic scattering. Certain restrictions were placed to keep from overloading the measuring capacity. These restrictions were made as general and absolute as possible to avoid introducing any bias into the finding of events. Examples of the type of restrictions introduced were that:

(1) one outgoing track had to lie on each side of the incoming track;

(2) the included angle between the two outgoing tracks had to be less than 180 deg;

(3) the positive track could not be backwards with respect to the incoming track;

(4) there was a simple criterion for rejecting events which were far out of coplanarity;

(5) neither track could show a π-μ-e decay point, since the lowest energy-scattered pion still had enough energy to traverse the entire chamber; and

(6) there were some restrictions on the projected scattering angle of the pion with respect to the projected range of a stopping proton.

A separate scan card was made out for each picture containing an event. On the average, three events were measured in every five pictures. Many pictures had more than one event. Ionization was not used for identifying the events since there was too much variation for an absolute criterion. The main causes of variation were the relatively slow spill of the beam (about 2-3 ms) causing differences in ages of the tracks in one picture, and long-time drifts in the operating conditions of the chamber causing variation from picture to picture. The scanners noted when the recoil proton came to rest in the chamber, making a momentum measurement by range possible. The criterion for when a track was to be considered non-beam, and thus rejected, was not made definite and varied slightly from scanner to scanner. It always well exceeded restrictions placed on the incoming tracks after measurement, however, so no beam events were rejected at the scanning level by this lack. A list of all unusable pictures was kept.

At least two different scanners did substantial portions of each energy, reducing effects of personal bias for comparative purposes. One-fifth of the film was independently rescanned by the two most experienced scanners, to determine efficiencies of all scanners. The efficiencies are discussed in Sec. IV. In addition, for 40% of the rolls (a roll is 250 pictures long), a count of the number of tracks entering the scanning region and the total number of events occurring in it was taken for every tenth picture.

After a scan card made for an event, it was measured on a digitized microscope. Locations of a series of points on each track

were taken from the negatives of each view and punched directly on IBM cards. Most of the measurements were made on a motor-driven microscope with a servo-mechanism which centered automatically on the track. This device had the advantage that the entire picture was visible on a screen, reducing the number of operator errors in which the wrong track was measured.

Most of the subsequent data reduction and processing was done on an IBM 650 computer. Figure 2 shows the flow diagram of the data processing. The first program (FOG III) produced angles in space and momenta for each track. A coordinate system was used in which X ran the length of the chamber, Y across and Z up, to form a right-handed system. The series of X and Y locations from each view were first corrected for optical distortions of the chamber, which were mostly due to the presence of oil. Certain regularity tests were applied to reduce the effects of digitizer errors. The points from View 2 were interpolated to the same X's as the points from View 1, and the differences in Y were used to find the height, Z. Thus a series of X, Y, and Z points in space along each track were generated. A parabola was least-squares fitted to the rectangular projections of these points on the X-Y plane. A radius of curvature was found from the constants of the fitted parabola. The momentum was calculated from the curvature by using the magnetic field value at the center of the track. The azimuthal angle, β, was defined as the angle with respect to the +X axis of the tangent at the event to the circle projected on the X-Y plane. The dip angle from the +Z axis, α, was found by projecting the points in space onto a vertical plane parallel to the chord of the track, and fitting a straight line by least squares. The event was located and the lengths of the tracks were also found. Errors were assigned to α, β, and p, based on the sum of residuals of the least-squares fitting. A simple attempt to take multiple scattering into account assigned a 10% error to the momentum, to be added in quadrature to that from the residuals. No multiple scattering errors were assigned to the angles. Setting accuracy was not directly considered. These FOG III errors could only be taken as approximations.

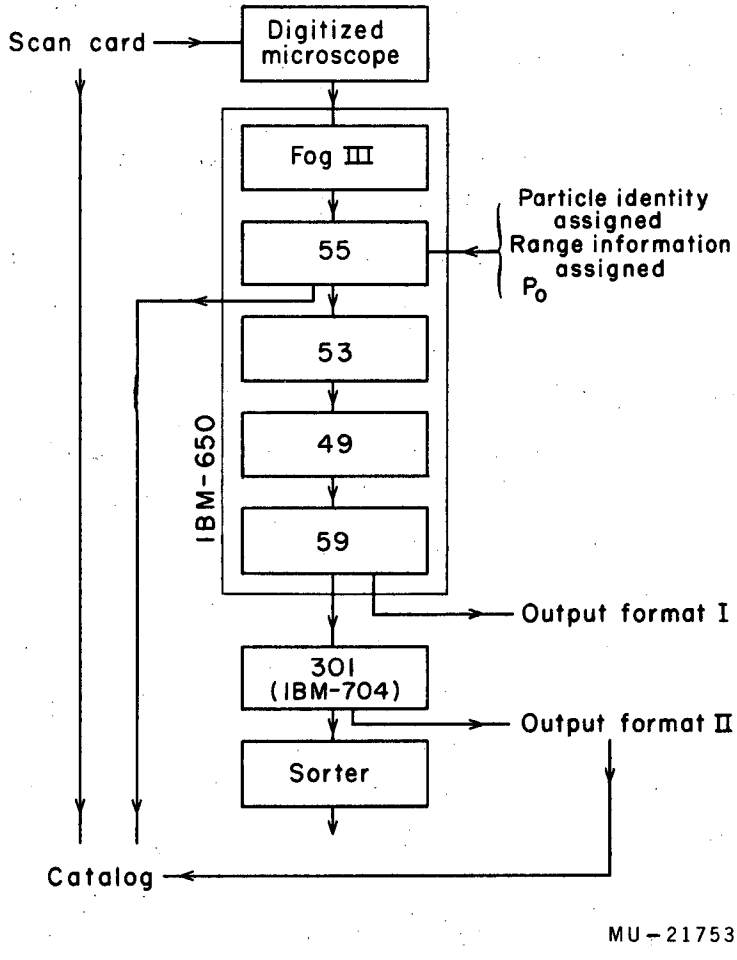

Fig. 2. Flow diagram of data reduction from scan cards to final output. The various programs are explained in Secs. II and III.

The incoming track of an event was extrapolated back to the thin window of the outer pressure vessel by Program 55. The Y and Z at that location had to fall within regions somewhat less than the actual size of the thin window (the thin window being actually divided into three parts by support bars). Also the azimuthal angle had to be within $\pm 5°$ of the X axis, and the dip angle within $\pm 3°$ of horizontal. These precautions were taken to insure that all tracks used had the proper momentum within the 1.5% spread. The thick part of the outer pressure vessel corresponded to about 100-Mev energy loss. The angle requirements tended to insure that the tracks had not scattered from any collimator or magnet. An output page indicated whether an event was accepted or rejected by these beam criteria. Identity of the tracks was assumed at this point based on tracks 0 and 1 being pions, and track 2 the recoil proton. Scanners were instructed to use these numbers on the scan cards. This procedure avoided the necessity of separate supplementary information sheets for each event. If the proton stopped the information was added here, and for appropriate events a momentum measurement by range replaced the measurement by curvature. The momentum of the incoming track was assigned from the known beam momentum, position, and energy loss in the chamber.

Fitting a circle to a track gives the momentum at the center of the track length. A correction for energy losses of the outgoing tracks (except range measurements) from the origin of the event was made by Program 53.

The first kinematical program (Program 49) was a constraints program[17, 35, 36] which adjusted the parameters of each event relative to their FOG III errors, so as to make the event elastic. Since the constraints were non-linear, a linear approximation (Taylor expansion) was used and the process iterated three times. In an elastic event with nine parameters measured, four independent quantities may be specified by five others, and momentum and energy conservation. These four were taken to be transverse and longitudinal momentum balance, coplanarity "volume" (the triple scalar product of unit vectors in the directions of each track), and the energy balance. All these quantities

(called F_1, F_2, F_3, and F_4) are zero within measurement errors for an elastic event. The F's were given in the output, before each step of the constraint and after the last. How well any event fitted the assumption of elasticity was indicated by M*, which was χ^2 for the adjustment, plus twice the sum of the deviations from zero of the F's after the third iteration. The amount that each parameter was adjusted was given in the output. While M* gave a useful preliminary idea whether an event was elastic, it was not considered completely correct since FOG III errors which entered as weighting factors were only approximate.

The next kinematical program (Program 59) assumed that the assigned incoming momentum and measured scattering angle of the pion were correct, and calculated the following:

(1) the difference between the measured proton recoil angle and that calculated for an elastic event (called $\Delta\theta_r$);

(2) the difference between the calculated momentum for an elastic event and the measured momentum divided by the calculated momentum for both outgoing tracks (called $\frac{\Delta p}{p}s$ and $\frac{\Delta p}{p}r$ for the pion and proton, respectively); and

(3) the angle (ψ) that the recoil proton made with the plane of the two pion tracks.

In addition, the angle of orientation (ϕ) of the plane of the scattering with respect to the +Z axis, and the center-of-momentum system scattering angle (θ_s^*) and its cosine were calculated. The basic FOG III data and the angles the scattered pion and recoil proton (θ_s and θ_r) made with the incoming pion were given. The combined results of Programs 49 and 59 were printed in Output Format I. All investigations of identifying-events and error structure were made using this output.

After a detailed study of the errors present was made, another program was written to give the events a χ^2 test for elasticity. This is discussed in the following section. This program (301) was written for an IBM-704 computer. The magnitude of the vector unbalanced momentum was also calculated. The program also edited the data for ease of reading, prepared a summary card for machine sorting of the

events, and checked range assignments. The print-out was called Output Format II.

A catalog was kept to check on the events in the various stages of the data reduction. An entry was made from the scan card when an event was found. Whether an event was accepted or rejected by Program 55 was noted. The final entry was made when an Output Format II page became available for the event.

III. IDENTIFICATION

The principal task in any bubble chamber experiment is the identification of events. The problem in this particular experiment was to pick out the elastic interactions from all the non-elastic. In principle, the measuring of the three-vector momenta over-determines the elasticity of an event. In a propane bubble chamber the problem is complicated by the presence of carbon. A pion can interact with essentially only one proton of a carbon nucleus, and to knock it out so that the residual nucleus forms no tracks. Such a scattering, where the only non-elastic part comes from the binding and the internal motion of the proton, is called a quasi-elastic scattering. Protons are bound in carbon by only about 16 Mev, and have an approximate Maxwellian momentum distribution with a mean momentum of about 200 Mev/c. Thus a quasi-elastic scattering may approach the kinematics of an elastic event very closely. The identification is further complicated by the experimental uncertainties in the measured quantities. These experimental errors may be ascribed to two main causes: measurability, and multiple Coulomb scattering. The term measurability includes the error of not setting on the center of a track, errors in reading the position of a point (digitizer errors), the effects of turbulence in both propane and oil, and any remaining uncorrected optical distortions. Small angle ($\lesssim$ 2 deg) single Coulomb scatters, which are easily missed in scanning, also contribute to the experimental errors. Typical values for the combined errors in the experiment at hand are about 0.3° in β, 1.0° in α, and 100 Mev/c in momentum. A careful study of the error structure is necessary to arrive at a non-subjective separation of the elastic events.

In a two-prong event (one incoming track and two outgoing tracks) nine quantities are measured: two angles and the magnitude of momentum for each track. Three angular quantities are needed to specify absolute orientation in space. Thus six variables are available for identifying the event. The conservation of energy and momentum give four equations coupling these six quantities with the two masses involved. If any four are specified, the other four may be found by

solving the equations. These four then may test the assumption of elasticity. Many different sets of variables may be used. It is usual to specify the masses, since the identities of the incoming and struck particles are known. Two such sets (the F's; and $\Delta\theta_r$, ψ, $\frac{\Delta p}{p}$ s, $\frac{\Delta p}{p}$ r) were specified in the previous section. Each variable of both sets is zero within errors for elastic events. The first named set (hereafter called the "F set") is of a form following directly from the conservation equations; the masses, and scattering and recoil angles, are specified. The second set (hereafter called the "delta set") is more directly related to the measured quantities; the masses, initial momentum, and pion scattering angle are assumed. Neither of these sets has really independent components. An error in any of the directly measured variables will be reflected in several of the components of either set in most cases. An error in any of the momenta will show up in three of the F's. An error in either of the two outgoing momenta shows up only in the appropriate term in the case of the delta set, but an error in the initial momentum is reflected in three of its terms. However, the initial momentum is well known, and coupling to the $\Delta\theta_r$ term is weak. An error in any of the measured angles shows up in three of the F's, while such an error is reflected in two or four of the terms, depending on which angle it is, for the other set. As a first approximation, the terms of the sets may be regarded as independent. That this approximation is indeed a good one, was later verified for the delta set. The directly measured quantities (α, β, p), independent to a higher degree, were not used because of the cumbersome equations relating them to the angles in the conservation equations.

Histograms of each component of both the F and delta sets were made with a sample of the events. All studies of errors and identification methods were made with samples of a few hundred random events. Most were done with one energy, and the energy dependence checked later. The histograms all peaked strongly around zero, but dropped off more slowly than a normal (Gaussian) distribution to an almost constant background. Since angles are relatively better-measured than momenta, and since two of the components of the delta set depend

essentially on angles only, while only one of the F set components depends on angles only, all subsequent work was done with the delta set, with one modification as noted below. The decision to use the delta set was also based on its closer relation to the measured quantities.

The process of arriving at the final form for the identification of elastic events (Program 301) could best be described as "iterative cuts with feedback." Rough limits were placed on one or more of the variables of the delta set, which would eliminate some of the non-elastic events. This enriched sample then showed more clearly the spread in the other variables due to experimental errors, since the spread due to non-elastic events was reduced. A better notion of the errors resulted which could be used to obtain a more nearly elastic sample, and so on. A scatter diagram of ψ vs θ_s for selected events showed that ψ was much more poorly determined for small scattering angles. A similar plot of F_3 showed that it was essentially independent of the scattering angle. So F_3 was substituted for ψ in the delta set. The two were related by the relation $F_3 = (\sin\psi)(\sin\theta_s)$.

The accuracy with which each of these variables is measured differs from event to event, depending on the lengths and momenta of the tracks, and the orientation of the event in the chamber. Scatter diagrams of $\Delta\theta_r$ vs θ_s or ℓ, $\Delta p/p$ vs ℓ or p, and so on, for partially selected events, revealed that simple cuts naturally could not give a proper identification of elastic events. Examination of histograms for all values and for restricted ranges of ϕ, the angle of orientation of the plane of scattering with the Z axis, showed that measurement errors did not depend strongly on ϕ. This dependence was therefore ignored until later. F_3 was found to be sufficiently independent of configurations and sufficiently close to being normally distributed that a constant standard deviation could be assigned for it. The standard deviation for F_3 was 0.015 in unit-lengths cubed. The functional dependence of the standard deviation of $\Delta\theta_r$ could be expressed as a function of the scattering angle to good approximation. The standard deviation increased for small θ_s, and went to a constant (0.8 deg) for θ_s (lab) greater than 70 deg.

The error analysis for momenta started from theoretical guides. Expected errors were first assumed due to two components, multiple scattering and measurability, which could be added in quadrature. Multiple scattering was taken directly from theory relating the error in curvature measurement to the rms scattering angle.[37, 38] The rms scattering angle was found from the leading term of Molière's theory,[39] with energy losses neglected. The contribution of only the carbon in the propane was considered, since that of the hydrogen is negligible in comparison. The effect of these simplifications is small except for particles near the end of their range. Since stopping protons had their momenta measured by range instead of curvature, and since the pions from elastic events never stopped in the chamber, the overall approximation is good. Careful note had to be made of the distinction between a track in space and its projection on the X-Y plane.

Both multiple scattering and measurability errors produce symmetric errors in the sagitta of the curve. Since curvature and the sagitta are directly proportional to each other for fixed track length, the error will be symmetric in curvature. Since momentum goes inversely with curvature, the errors in momenta will not be symmetric. A large positive error in momentum is more likely than a large negative one. If one defines $\frac{\Delta c}{c}$ in a similar manner to $\Delta p/p$ (Sec. II), then they are related by

$$\Delta c/c = 1 - (1 - \Delta p/p)^{-1}$$

If it is assumed that the error in curvature from measurability is due to a normally distributed error in sagitta, then the standard deviation in $\frac{\Delta c}{c}$ is proportional to $p\ell^{-2} (\sin \alpha)^{-1}$. The $(\sin \alpha)^{-1}$ comes from projecting on the X-Y plane of the film. A scatter diagram of $\ell^2 \left| \frac{\Delta c}{c} s \right|$ vs $\frac{p(\text{measured})}{\sin \alpha}$ was made for the scattered pions from events thought to be elastic and hence having known momenta. This form of plotting was chosen since multiple scattering has a very small effect on such scatter diagrams. An analytic expression for the standard deviation due to measurability was found, to which the scattering term was added in quadrature.

A constant standard deviation of 0.05 could be assigned for $\frac{\Delta p}{p}$ r

when the momentum was measured by range. No dependence on track length was found, contrary to what might be expected. This fact may be understood in terms of the uncertainty in p_o and θ_s, which enters into $\Delta p/p$.

The distributions in the four variables of the modified delta set were thus found to be approximately normal when the standard deviations were given the proper functional form. If normal distributions and statistical independence are assumed, then a χ^2 test for elasticity may be given. The equation giving χ^2 is

$$\chi^2 = \sum_{i=1}^{y} (x_i)^2$$

where x_i stands for one of the variables divided by its error.

χ^2 was calculated by hand for a number of events. A cut was made where the inelastic tail to χ^2 began. Histograms of the x_i for the elastic events were approximately normally distributed as expected. Through the use of scatter diagrams, corrections were made to the standard deviations and a ϕ and ℓ dependence to F_3 and $\Delta\theta_r$ was added. The assumption of statistical independence was sufficiently verified with further scatter diagrams of one variable against another, which showed little correlation.

The standard deviations, which had largely been graphical, were fitted with analytic functions suitable for computer work. After a sample of events was run through this program (301), the results were again checked and small changes made in some constants. The functional forms of the standard deviations which were finally used were:

$$\sigma_{F_3} = 0.016 \left(1 + \frac{2}{0.6 + \ell_r^2}\right) (1 - 0.28 \cos 2\phi)$$

$$\sigma_{\Delta\theta_r} = \begin{cases} 6.10\ (\theta_s)^{-1/2}\ (1 + 0.09 \cos 2\phi)\ \left(1 + \dfrac{1.6}{2 + \ell_r^2}\right) & (\theta_s \leq 70°) \\ 0.73\ (1 + 0.09 \cos 2\phi) \left(1 + \dfrac{1.6}{2 + \ell_r^2}\right) & (\theta_s > 70°) \end{cases}$$

$$\sigma_{\frac{\Delta c}{c}} = \frac{1}{\sin \alpha}\left[\left(\frac{0.36}{\beta\sqrt{\ell}}\right)^2 + \left(\frac{26.2\,p}{\ell^2+25}\right)^2\right]^{1/2} \qquad \text{(for curvature)}$$

$$\sigma_{\frac{\Delta c}{c}} = 0.04 \qquad \text{(for range)}$$

In the above, ℓ is in cm, θ_s is the laboratory angle of the scattered pion in degrees, p is in Bev/c, and $\beta = v/c$. The same form was valid for $\frac{\Delta c}{c}$ for both pions and protons through the use of β. A sagitta error due to measurability of 0.012 cm in space may be deduced from the equations for $\frac{\Delta c}{c}$. This value may be compared with the sagitta error of 0.027 cm found by Thomas in an earlier run.[36] The main reason for improvement is probably due to the reduction of oil turbulence.

Histograms of χ^2 and x_i for elastic events, at 610, 655, and 750 Mev are shown in Figs. 3a-b, 4a-b, and 5a-b, respectively. The theoretical distribution of χ^2 for four degrees of freedom is also shown with normalization to equal area for $\chi^2 \leq 11.0$. Agreement is quite satisfactory. A cut was made at $\chi^2 = 11$ to separate the elastic events. The location of the cut was chosen at the point where elastic events and non-elastic events had equal amplitude, assuming that the elastic events were following the theoretical curve. This choice minimizes the non-elastic contamination and the correction for elastic events beyond the cut. The inelastic tail, all of which is not shown, decreases steadily with increasing χ^2. About 40% of the events measured were elastic. Each of the x_i for elastic events should be normally distributed with unit variance. Such a curve is shown for comparison, normalized to the same area. The agreement is gratifying except for $X_{\frac{\Delta c}{c}\,r}$ by curvature, where the observed distributions are too narrow. This difficulty comes from the shorter proton tracks where errors on the order of several hundred percent are expected. A more detailed consideration of how FOG III fits the curves to the points would have to be made to get better agreement. Since the overall behavior of χ^2 is satisfactory, a more detailed analysis is held to be unnecessary.

Note that a shift from zero in the peak of $X_{\frac{\Delta c}{c}\,r}$ by range would

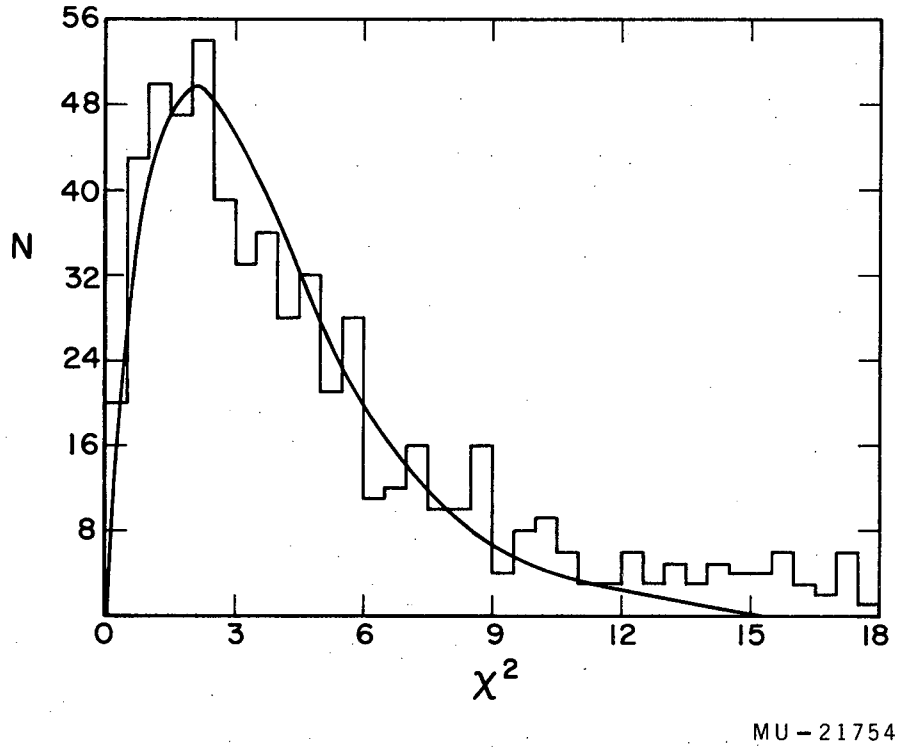

Fig. 3(a). Chi-square distribution at 610 Mev. The distribution extends well beyond the portion shown in the figure, dropping monotonically. The smooth curve is the theoretical distribution of χ^2 for four degrees of freedom.

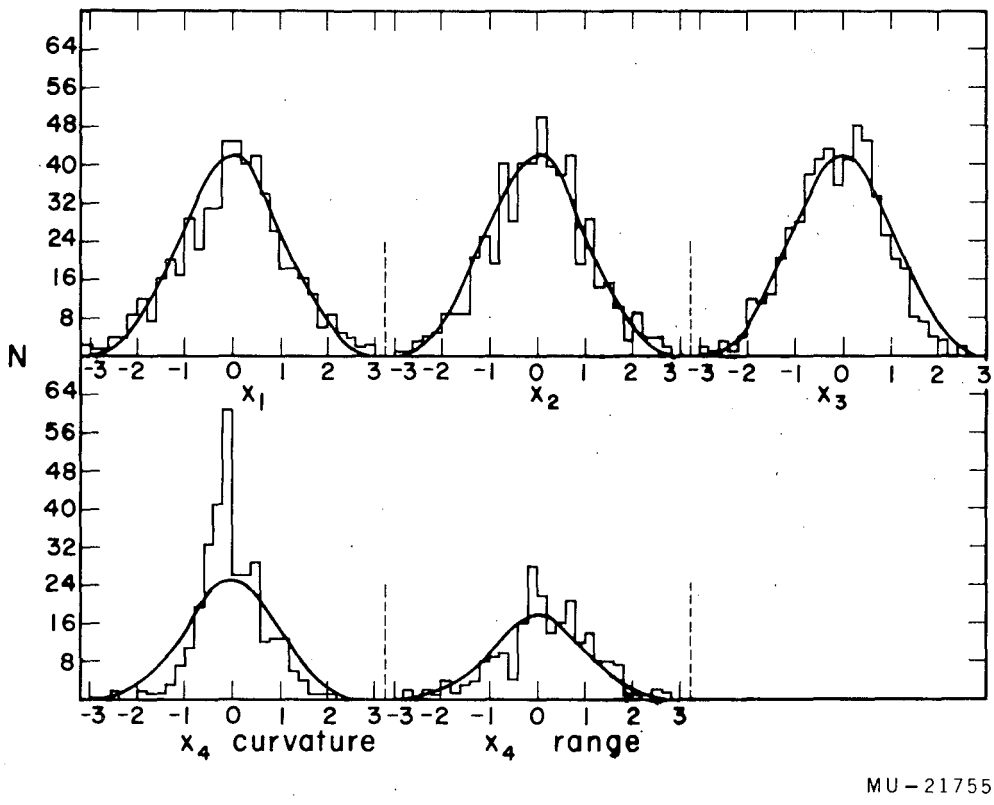

Fig. 3(b). Distributions at 610 Mev of the normalized variables (x_i) entering into χ^2 for elastic events. Subscript meanings: 1 = coplanarity (F_3); 2 = $\Delta\theta_r$; 3 = $\Delta C/C$ for pions; 4 = $\Delta C/C$ for protons measured both by curvature and range.

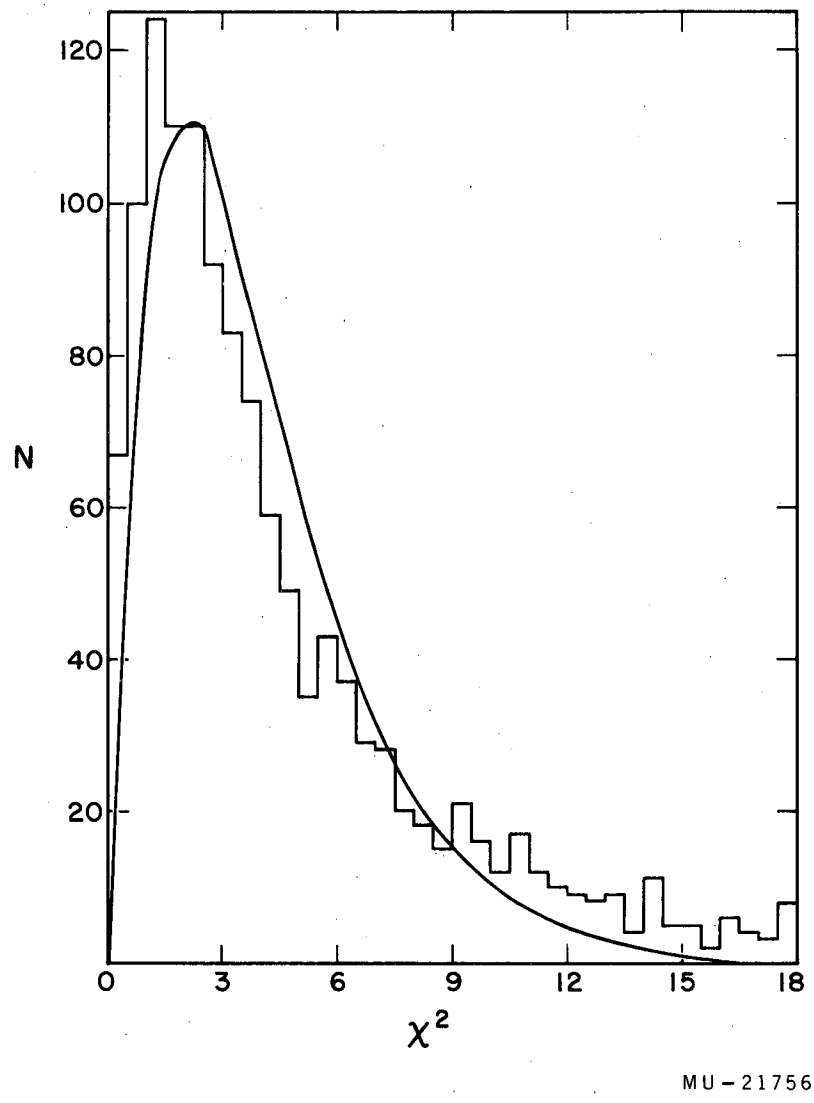

Fig. 4(a). Chi-square distribution at 655 Mev. The distribution extends well beyond the portion in the figure, dropping monotonically. The smooth curve is the theoretical distribution of χ^2 for four degrees of freedom.

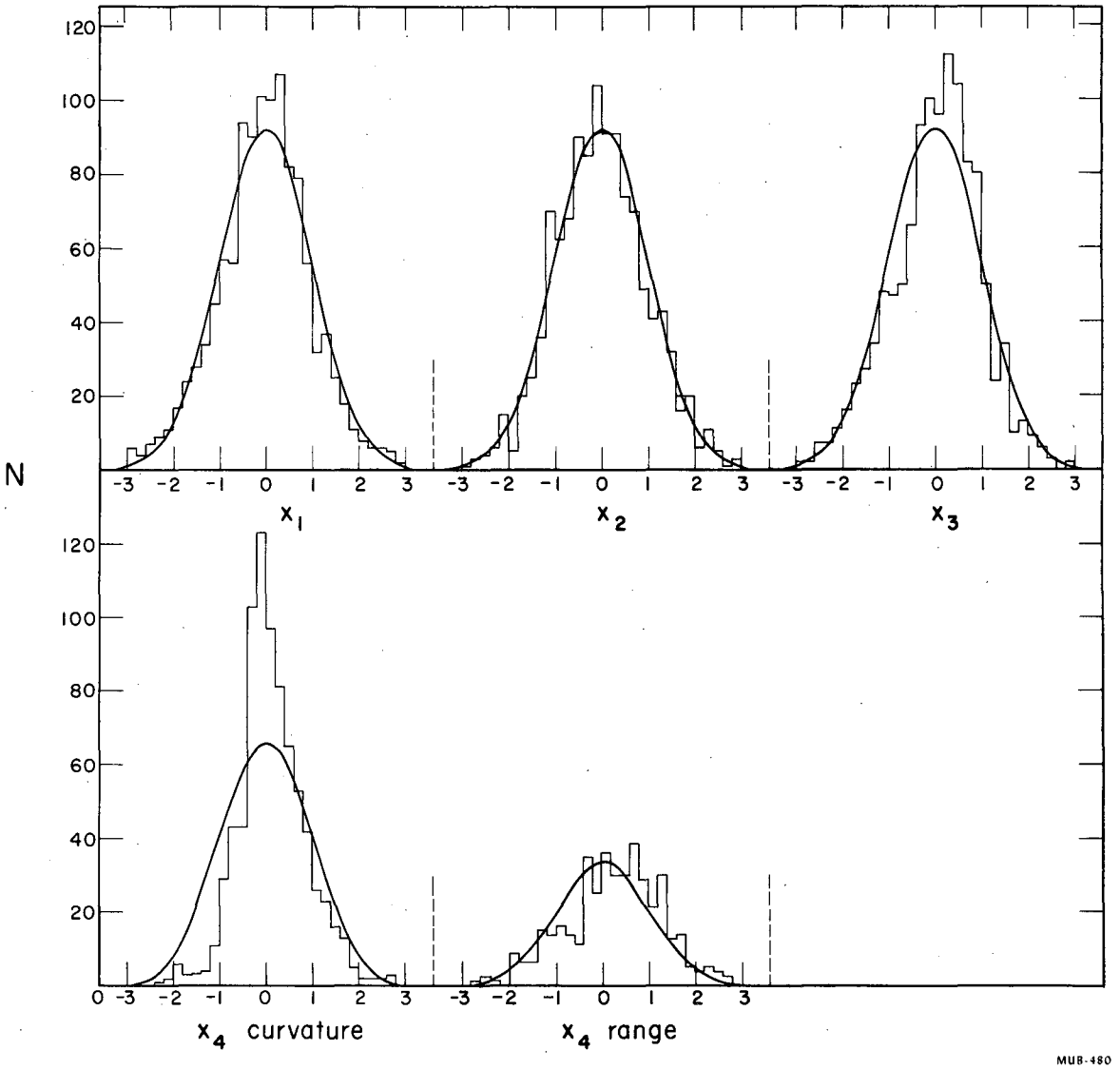

Fig. 4(b). Distributions at 655 Mev of the normalized variables (x_i) entering into χ^2 for elastic events. Subscript meanings: 1 = coplanarity (F_3); 2 = $\Delta\theta_r$; 3 = $\Delta C/C$ for pions; 4 = $\Delta C/C$ for protons measured both by curvature and range.

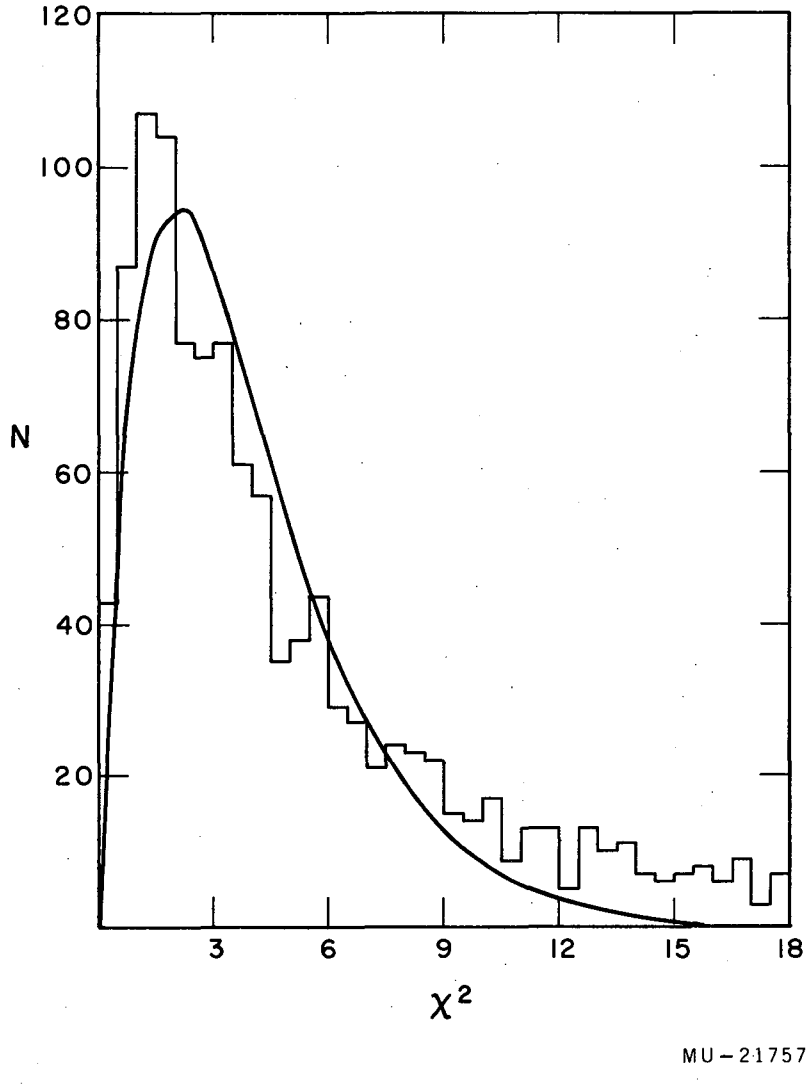

Fig. 5(a). Chi-square distribution at 750 Mev. The distribution extends well beyond the portion shown in the figure, dropping monotonically. The smooth curve is the theoretical distribution of χ^2 for four degrees of freedom.

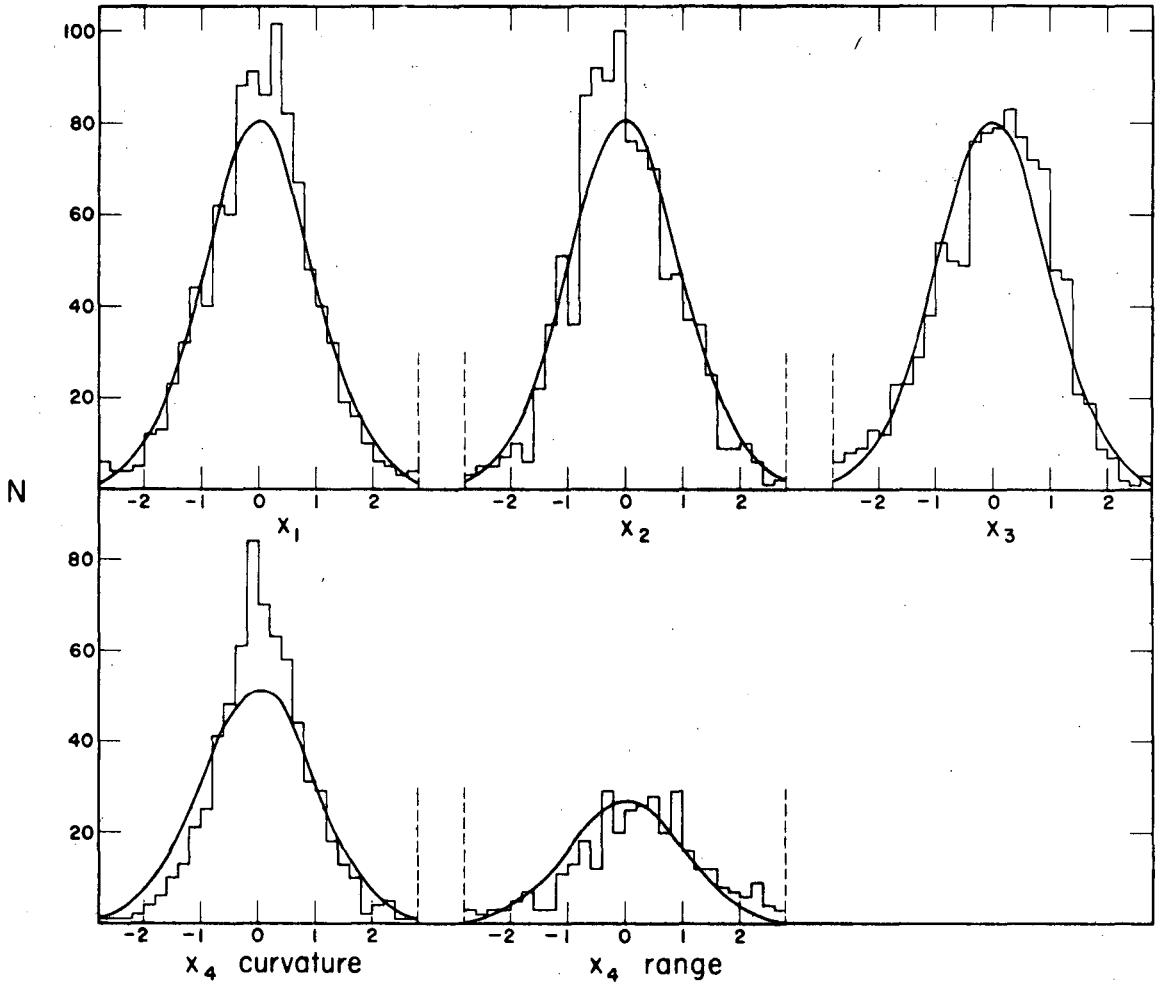

Fig. 5(b). Distributions at 750 Mev of the normalized variables (x_i) entering into χ^2 for elastic events. Subscript meanings: 1 = coplanarity (F_3); 2 = $\Delta\theta_r$; 3 = $\Delta C/C$ for pions; 4 = $\Delta C/C$ for protons measured both by curvature and range.

be indicative that either the assigned p_o or the measured θ_s were systematically incorrect. A systematic error in θ_s appears unlikely, both from a general consideration and from the data. Small shifts of the peak of $X_{\Delta c r}$ to positive value by about 1/4-σ are suggested by the data. Since $\sigma = 0.04$ and since $\frac{\partial p_r}{\partial p_o} \simeq 1$ for small angles, this shift corresponds to too low a value for the assigned (wire orbit) p_o by about 1%.

IV. CORRECTIONS

It is necessary to make a number of corrections to the elastic events selected by the χ^2 program, in two categories: those arising from the difficulty of finding all interactions on scanning, and those from problems in identifying the events.

The difficulty of finding all interactions of a given type may be divided into a scanning efficiency consideration and a question of biases. The former is due to the scanner's inability to see all of the interactions defined in Sec. II without spending a prohibitive amount of time on each picture. It is necessary to establish with what efficiency the scanners find the events. Efficiencies are found from an independent rescanning of portions of the film. It is then assumed that the finding of events is a random process. That is, the second scanner will find the same percentage both of events the first scanner found and those he missed, and vice versa. The number of events that each scanner finds is proportional to his efficiency. The number of events of which each is found by both scanners is proportional to the product of their scanning efficiencies with the same constant of proportionality. From these three equations, the efficiency of each may be found. For this purpose, 20% of the film was rescanned. Ideally, the efficiency would be computed only for those events found to be beam elastic events. For example, if one scanner were much more conservative and put down almost all two-pronged events, he would appear to be more efficient than another scanner who discriminated against those events which did not satisfy all the scanning criteria. It was not possible to check scanning efficiencies for only beam elastic events at the time of writing, since an insufficient number of the events which were found on the second scanning had been processed. Efficiencies had to be checked directly from the scanning level. A check was made to see if difficulties as noted above could be biasing the estimate of the efficiency. The ratios of the beam-track events to the total number of events submitted, and the ratios of the elastic to beam events, were compared for the various scanners. These ratios were within expected fluctuations of each other, indicating that all scanners were closely following the instructions. Since these ratios

are about constant, a direct comparison of the events found in the various scans should be valid. Efficiencies were computed on a roll to roll basis. Efficiencies of all the rolls of a given (first) scanner at one energy were averaged. An error was assigned to the average efficiency from the sum of the squares of the deviations, from the average according to the usual prescription of statistical theory. The efficiency for a given energy was just the average of the efficiencies of the various scanners, weighted according to the number of rolls done by each. The average error was found in similar fashion. That the rolls which had been scanned twice had the combined efficiency of both scanners was taken into account. The statement of all corrections and estimated errors on the corrections is made in Table I. The observed number of events is divided by the given efficiency to correct for the scanning inefficiency.

In addition to the random scanning inefficiency there are certain systematic biases affecting all scanners. One of these biases is the azimuthal bias, due to the scanner's inability to find events whose plane of scattering is nearly vertical. The actual number of scatterings must be isotropic with respect to the azimuthal angle ϕ. The bias is easily detected by comparing the number of events in different intervals of ϕ. No systematic differences were found from one quadrant to another, so the distribution was folded into one quadrant to improve statistics. The events were first divided in various intervals of $\cos \theta^*$: $1.0 - 0.9$, $0.9 - 0.8$, $0.8 - 0.7$, $0.7 - 0.4$, $0.4 - 0.0$, and negative values. The histograms are shown in Figs. 6a-c. In the figures, 0 deg is the vertical and 90 deg the horizontal. The correction was determined by first averaging over that portion of the histogram near 90 deg which appeared uniform. The difference between that average and what was observed in the other intervals is the number of events lost. The error to the correction was estimated from the statistical error expected for the number of events in the biased and unbiased portions of the distribution. An error of 5% was assigned to the cases which appeared reasonably isotropic, to be conservative. The corrections were expressed as percentages and were applied to each interval of $\cos \theta^*$ in the angular distribution before summing for the total cross section. For $0.7 \geq \cos \theta^* \geq 0.0$ at 655

TABLE I

Corrections to the data expressed in %. A correction of 6 ± 2% means the data are either multiplied or divided by (1.06 ± 0.02) as the case may be. The data are divided by the scanning efficiency.

Energy in Mev	610	655	750
Scanning efficiency	78.4 ± 4.3%	88.1 ± 3.3%	83.3 ± 5.4%
Azimuthal bias			
$1.0 \geq \cos\theta^* \geq 0.9$	68.2 ± 12.3	43.7 ± 7.1	58.5 ± 10.8
$0.9 \geq \cos\theta^* \geq 0.8$	27.8 ± 8.8	9.2 ± 3.5	15.2 ± 4.9
$0.8 \geq \cos\theta^* \geq 0.7$	0.0 ± 5.0	2.5 ± 2.3	0.0 ± 5.0
$0.7 \geq \cos\theta^* \geq 0.4$	3.8 ± 2.4	0.0 ± 5.0	0.0 ± 5.0
$0.4 \geq \cos\theta^* \geq 0.0$	5.5 ± 3.1	0.0 ± 5.0	0.0 ± 5.0
$0.0 \geq \cos\theta^* \geq -1.0$	13.4 ± 7.3	6.2 ± 3.6	12.2 ± 2.4
Small angle scatters	11.9 ± 1.3	13.2 ± 2.0	10.9 ± 1.3
Carbon contamination	6.3 ± 2.1	5.7 ± 2.0	8.8 ± 2.2
Elastics beyond cut in χ^2	2.3 ± 1.0	2.3 ± 1.0	2.3 ± 1.0
X bias	9.8 ± 2.2	10.3 ± 1.5	17.8 ± 2.2
Events outside $27 \leq X \leq 73$ cm	1.7 ± 0	2.3 ± 0	2.7 ± 0
Events in process	20.5 ± 3.0	26.2 ± 3.9	14.5 ± 2.2
Rejects	2.9 ± 1.0	2.4 ± 0.6	1.7 ± 0.6
Proton range corrections	2.3 ± 1.0	1.7 ± 0.6	1.1 ± 0.5

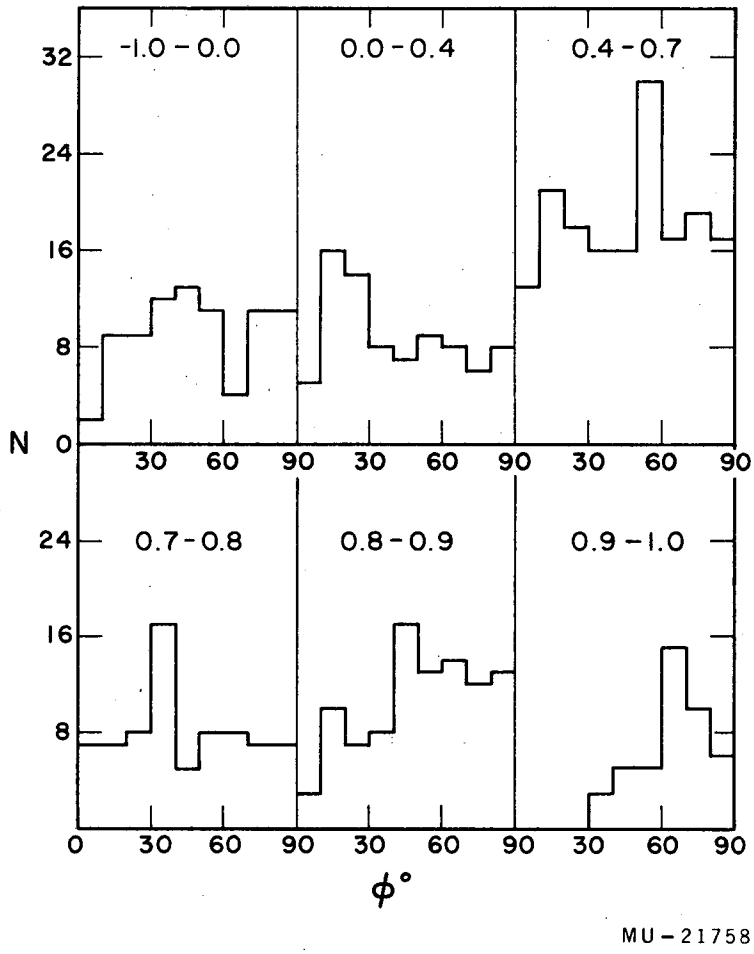

Fig. 6(a). Folded azimuthal distribution of the plane of scattering, at intervals of cos θ^*, for 610 Mev (0 deg is the vertical).

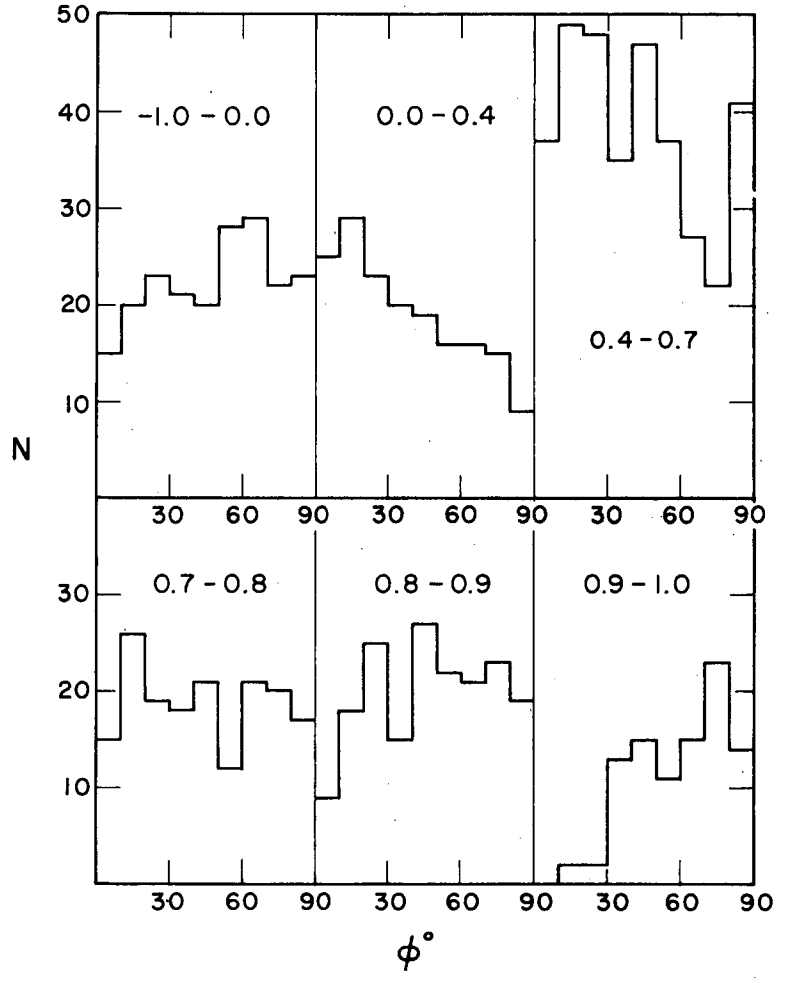

Fig. 6(b). Folded azimuthal distribution of the plane of scattering, at intervals of cos θ^*, for 655 Mev (0 deg is the vertical).

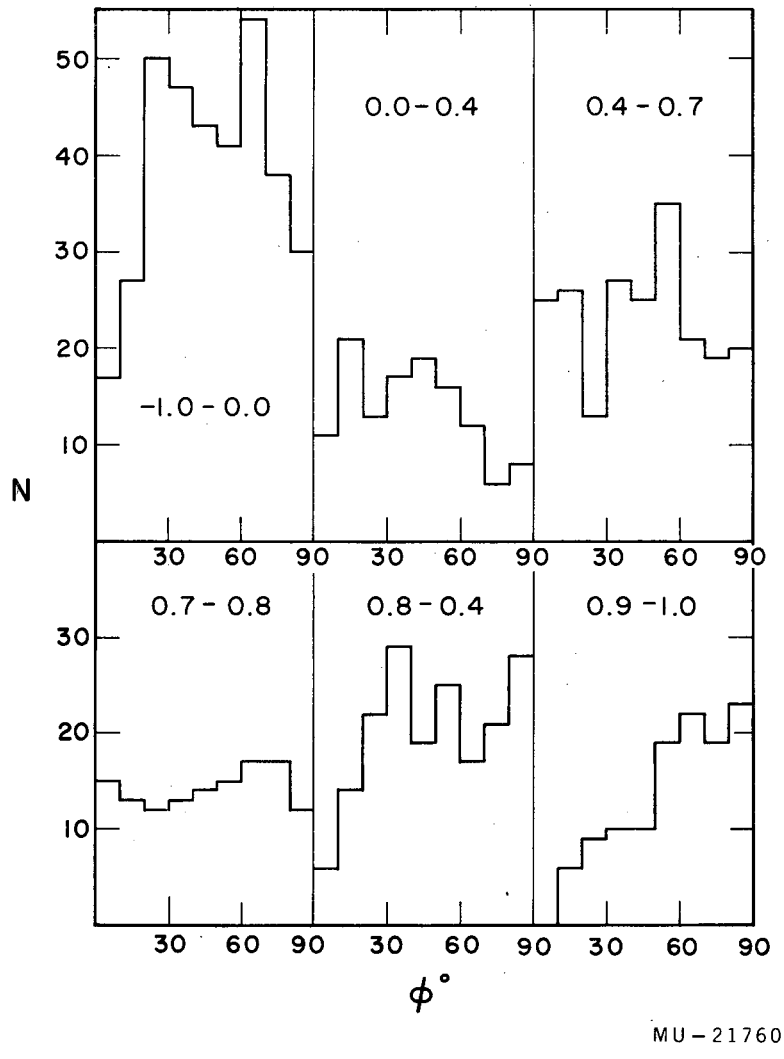

Fig. 6(c). Folded azimuthal distribution of the plane of scattering, at intervals of cos θ^*, for 750 Mev (0 deg is the vertical).

and 750 Mev, the azimuthal distribution dropped off towards 90 deg. Careful checks were made to see if this unexpected drop-off was caused by some part of the selection process. Plots of χ^2 for that angular interval for small and large ϕ were made. Azimuthal distributions of the inelastic events were drawn up. If the "missing" events had been misclassified as inelastics, they should have shown up in this study. No significant indications of such a misclassification were found. Also, a misclassification should be more systematic and tend to show at all intervals of $\cos \theta^*$ and all energies. It is very difficult to conceive of any scanning bias operating against such events. It is therefore concluded that, unlikely as it might seem, the drop-off towards 90 deg is due to a fluctuation. These intervals were given a correction of $0.0 \pm 5.0\%$ accordingly. If all of the lack of isotropy were to be due to some unexplained bias, then cross sections in the intervals of cosine from 0.7 to 0.4 at 655 and 750 Mev should be increased by about 10%, and in the intervals $0.4 - 0.0$ by about 20%. Note that the cross section is small in the last named interval, so that the absolute change would be small. A more detailed investigation of the behavior of these intervals was considered unjustified for the data at hand.

Another bias present was the missing of small-angle scatters. A pion scattering at less than about 10 deg in the laboratory has a recoil proton too short to be seen. For the angular distribution, all that is necessary is to ignore the angular region of $\cos \theta^* \geq 0.9$. A correction is needed for the total elastic cross section. The differential cross section at 0 deg may be calculated from the total cross section, the optical theorem, and dispersion relations. See for example Ref. 1. The latest total cross sections[12, 13] and the recent dispersion calculations based on them[40] were used. A linear extrapolation from the observed differential cross section outside of the forwardmost interval to the calculated value at 0 deg was made for each energy (See Sec. VI and Fig. 11). The area between the extrapolated line and the observed distribution gave the correction. An error was estimated from the uncertainty in making the extrapolation.

An example of an error in identification for which a correction must be made is found in the carbon contamination. As noted in Sec. II, a scattering on a proton bound in carbon may simulate a scattering from a free proton. In a certain fraction of cases, even a detailed selection criterion will be unable to distinguish these quasi-elastic scatters from true elastic scatters. One method of estimating the percent of the events called elastic which are actually on carbon is from the behavior of the χ^2 distribution used to select the events. The tail to χ^2 beyond the elastic events is assumed to be due to quasi-elastic events. This tail is then extrapolated under the elastic portion. The quasi-elastic part must certainly go to zero at $\chi^2 = 0$, also. The exact form for the extrapolation were not known, so a linear one to zero from the level of the inelastic part of the tail in the region of $\chi^2 = 11$ was made. The quasi-elastic distribution must be dropping off in some similar fashion, as shown by the following argument. If distributions of the various x_i in χ^2 are made for the inelastic events, the quasi-elastic parts of the distributions are, crudely, Gaussians with widths on the order of 2 or 3 times that of the elastic events. Chi-square for these events should then peak between values of 15 to 30, dropping to 0 for smaller values. This model is certainly too crude to be taken exactly, as the distribution shows no secondary peaking, but it seems sufficient justification for the linear extrapolation, since χ^2 for four degrees of freedom rises approximately linearly at first. The error to the correction was estimated from the uncertainty in the height from which to start the extrapolation to zero. This method of estimating the contamination yields a result of about 6%. Thomas found a value near this number.[36] Another method of estimating the contamination has been used by workers using other propane chambers.[18, 41, 42] It assumes that the density of coplanar quasi-elastic events should vary smoothly on a θ_s vs θ_r scatter diagram in the vicinity of the area accepted for elastic events. If there are fewer background events in the area covered by the elastic region than in a similar area on each side of the elastic region, then the ones missing are presumed to be quasi-elastic events incorrectly identified as elastics. A somewhat similar procedure was used in this experiment as a check.

The distributions of $\Delta\theta_r$ for inelastic events with $|F_3| \leq 0.05$ were found. They are shown in Fig. 7. The distributions of background events are expected to go through a maximum at $\Delta\theta_r = 0$. A smooth curve was drawn representing approximately the expected background. The area missing under this curve is the amount of contamination to the elastic events. The contamination found in this manner was only from 1 to 2%. If these later figures are correct, it becomes difficult to explain the size of the tail to the χ^2 distributions immediately beyond $\chi^2 = 11$. However the amount of disagreement between the two methods is not really significant. The former figures were used.

A cut was made at $\chi^2 = 11$ to select the elastic events. If the elastic events are following the theoretical curve in this region (which seems probable), then, as Figs. 3a, 4a, and 5a show, a certain number of elastic events lie beyond this cut. The area of the theoretical curve beyond $\chi^2 = 11$ is 2.3% of the rest. An uncertainty of ± 1% was attached to this correction to allow for some variation from the expected curve. Note that if the lower carbon contamination of the second method given above is correct, then there is a certain doubt as to whether the elastic distribution continues to fall off as expected. The lower contamination figure would indicate the assumptions of the linear extrapolations method as incorrect. Accordingly, the elastic distribution would extend beyond $\chi^2 = 11$ with a greater amplitude than expected. No quantitative estimation of this possible effect is given.

Another correction was made for a bias in the X distribution of the events. This bias was thought to be due to data reduction rather than scanning, as pointed out below. The number of events as a function of X should fall off exponentially with a decay length equal to the mean free path for <u>all</u> interactions in propane. Histograms of the elastic events as a function of X are shown in Fig. 8. The expected exponential decay is shown, normalized to the average of the central 20 cm, and using the mean free path lengths given in Sec. V. Only the region from 27 cm to 73 cm was used. It may be seen that the beginning and end regions are systematically below the expected line. Similar plots of the inelastic events did not show the same losses. Checks of the measuring process were made by reprojecting some of the events with an oil tank which

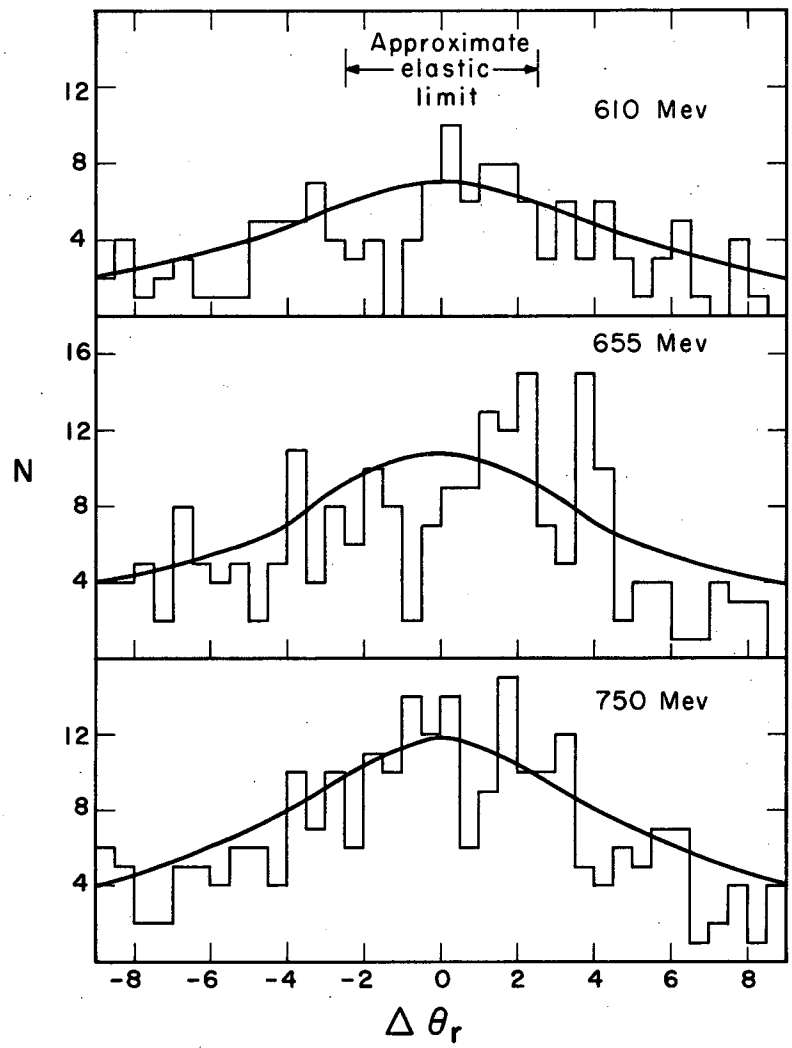

Fig. 7. Distribution of the coplanar inelastic events in $\Delta\theta_r$. The smooth curve is the approximate expected behavior. The area between the smooth curve and the observed histogram is an estimation of the carbon contamination to the elastic events.

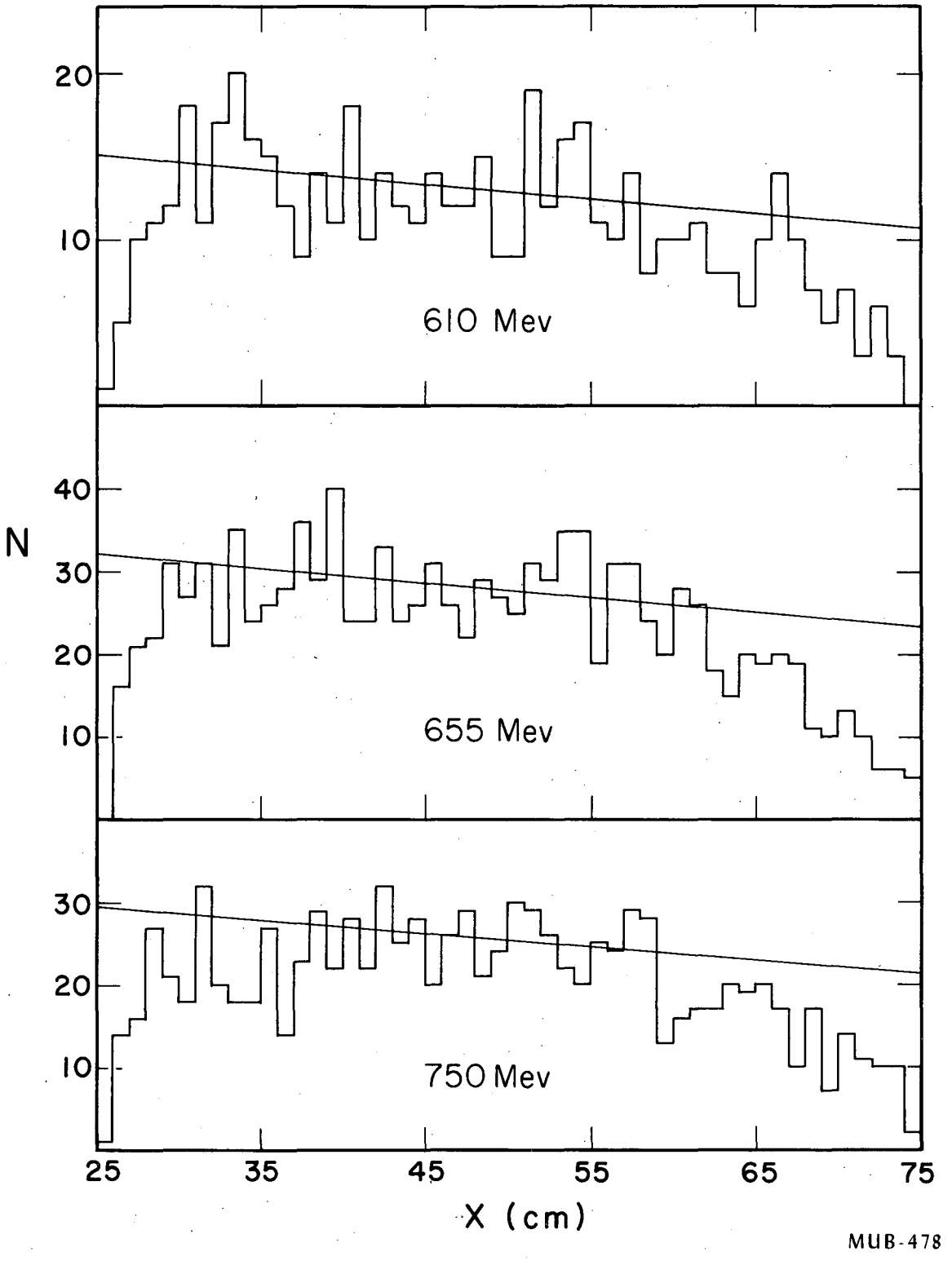

Fig. 8. Distributions of the elastic events as a function of X (the longitudinal direction in the chamber), at 610, 655, and 750 Mev. The smooth curve is the expected attenuation due to interactions of the beam.

removed the optical distortions due to the oil. The two stereo views of the events were then recombined on ground glass and the events measured in space. In the sample checked, about the same percentage of events were found to have been measured incorrectly, and thus wrongly called inelastic, as the percentage of events found missing from the X distribution. Also, the X distribution of events incorrectly measured corresponded to the areas from which events were missing, in the distributions of the elastic events. These facts were taken to indicate that the bias was due to measurement. Most events missed were at the exit end of the chamber where turbulence was greatest, making tracks difficult or impossible to measure. A small amount of drop-off was probably due to the beam beginning to be bent out of the chamber through a side wall. The corrections were found from the areas between the expected and observed curves. The errors on the corrections are from the statistical errors associated with the events present in the biased regions. The angular distributions of the elastic events for different regions of X were the same within statistics, demonstrating that the events which were missed were randomly distributed in angle. The few events lying outside of the region $27 \leq X \leq 73$ cm were included in the cross sections. Corrections were made to the normalization to account for them.

A final correction must be made for events which have not finished passing through the data-reduction process. FOG III applies a regularity test to be the series of points measured along each track. A certain fraction of the events fail this test because of digitizer errors. Various operator mistakes may be detected also. Events that fail to pass through FOG III have to be remeasured. Some events have been measured as many as five times. Cards may be lost between the various stages of the data reduction, or may have gotten out of order so as to be unusable by the next program. A small percentage of the events still have not been fully processed.

The catalog described in Sec. II keeps track of events as they pass through the various stages. Process failures may be noted at two points: Program 55 and final output. The number of events which had not gone through Program 55 was multiplied by the fraction of beam tracks for events which had passed Program 55 and by the fraction of elastic events

observed in the data which was returned, to arrive at the number of missing elastic events. Events passed by Program 55 as beam-track events, but not arriving in the final output, were multiplied by the fraction of elastic events out of all the beam events. Errors to these corrections were estimated to be about 15% of the correction, which allowed both for statistics and for uncertainties in the various ratios used. A small number of events were rejected as being unmeasureable. These rejects were assumed to have the same portion of elastic events as events not rejected. A small correction was made for those events for which the scanner had incorrectly called a proton which left the chamber as a stopping proton.

A few further comments on the validity of the identification process may be made. The M* selection mentioned in Sec. II may be used to select the elastic events alternatively to the χ^2 program. Such a selection gives 8%, 1%, or 3% more events at 610, 655, or 750 Mev, respectively. The angular distributions derived are perfectly compatible with those from Program 301, except for being slightly higher at the forward angles. It should be remembered that M* is based on only approximate errors for variables. Accordingly, the differences are not held to be important and mention is made only to show the degree of independence of the data to the exact selection method. The results of the χ^2 program are felt to be the better. The possibility that the tail of the χ^2 distribution beyond 11 may contain mostly elastic events for an interval has been suggested above. If such were the case, the shape of the differential cross sections would not change, since the angular distribution of the events $11 \leq \chi^2 \leq 30$ is the same as for $\chi^2 \leq 11$ within errors. Indeed, the shape has not changed grossly even by $\chi^2 = 100$. Another check on the separation of the events is found by comparing the histograms of p-unbalanced (the magnitude of the vector difference between the incoming and outgoing momenta) for the elastic and inelastic events, as shown in Fig. 9. In these figures, only events with tracks long enough for good momentum measurements (or proton ranges) were used. The difference is evident. The widths, shapes, and locations of

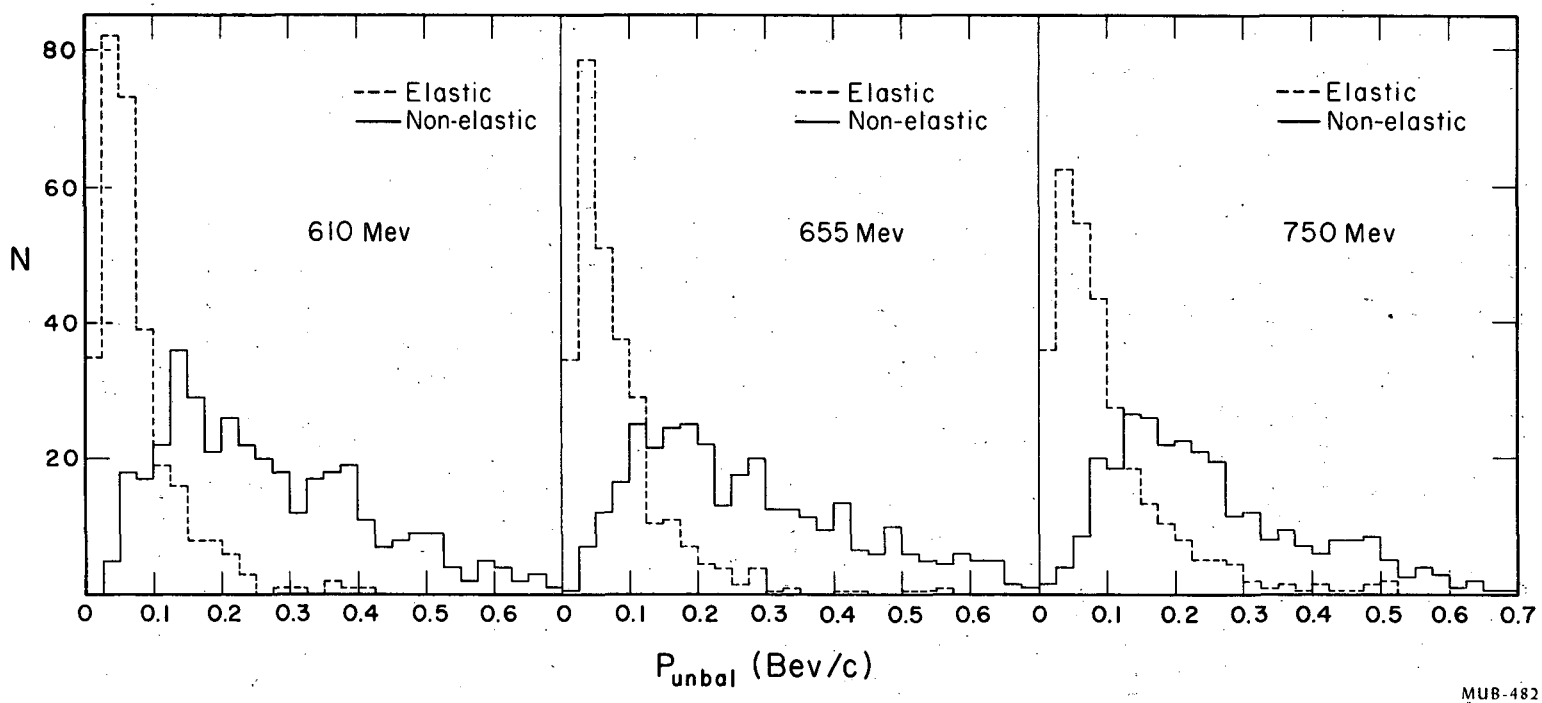

Fig. 9. Histograms of $p_{unbalanced}$ for elastic and inelastic events at 610, 655, and 750 Mev.

the maxima for the inelastic distributions are compatible with those expected for a Fermi momentum distribution in carbon, with experimental resolution and some pion production included. The diagrams are included as a qualitative indication of the separation of the carbon events from the hydrogen events.

A summary of all corrections is given in Table I. A correction of $6 \pm 2\%$ means that the data is to be multiplied or divided by 1.06 ± 0.02, depending on whether it is a positive or negative correction, except for the case of the scanning efficiency as already noted.

V. NORMALIZATION

To get from a (corrected) observed number of events to a cross section in mb, the track length of the pions and the density of hydrogen in propane must be known. A density of 0.415 gm/cc ± 2% was assumed for the propane (C_3H_8). For the former, the number of tracks entering the scanning region was counted in 4% of the film. Unless unacceptable, every tenth picture, was counted in 40% of the rolls. The track count was made during rescanning. The same criteria for when to count a track were used as for when to accept an event for measuring. Although the criteria were not precisely spelled out, various checks showed that the scanners were within a few percent of each other in accepting tracks. A few rolls were counted twice. By examining the differences between the two counts, an estimation of the efficiency for track counting could be made, similar to that for scanning for events (Section IV). The efficiency was 98 ± 2%. The average number of tracks per picture in each roll counted was found. Linear interpolations were made for the rolls between those rolls counted. The variation of the average beam flux with time was reasonably smooth. The average number of tracks per picture in each roll was multiplied by the actual number of good pictures in that roll, to give the total number of tracks in each roll. Only events with $27 \leq X \leq 73$ cm were used for normalization, giving an interaction volume 46 cm long. Not all tracks which enter the interaction volume traverse its entire length, because of interactions which attenuate the beam. Let λ be the mean free path for all interactions in the propane, and ℓ_o be the length of the volume (46 cm in this case). The average length a track goes, L, is given by

$$L = \lambda \left[1 - \exp\ (-\ell_o/\lambda) \right] .$$

The mean free path used was derived from the $\pi^- - p$[12, 13] and $\pi^- - C$[43] total cross sections. Interpolations between the measured carbon cross sections of Cronin et al. were done with an optical-model calculation similar to that used by the same authors. The mean free paths are on the order of 150 cm, so that the correction is small. Accordingly, a 15% error in λ makes only about a 1.5% error in L. The total track length is the sum of the tracks in each roll times L.

Only some of the tracks thus found came through the thin window within the required angular spread. It was assumed that the same ratio of beam tracks to non-beam tracks held for all tracks counted as for those with measured events. This assumption was checked partially by comparing the distributions of projected angle that tracks make with a fixed line at X = 25 cm for tracks with two-pronged events and for all tracks included in a track count. The two distributions agreed with each other. The average ratio of beam events to all measured events for each energy was used. An uncertainty was estimated for this ratio based on the spread in the ratios between the various scanners. The ratios were 0.270 ± 0.025, 0.535 ± 0.015, and 0.565 ± 0.015, at 610, 655, and 750 Mev, respectively. The effect of beam misalignment at 610 Mev is quite evident. Finally, a correction was made for the muon and electron contamination, as calculated below.

The muon contamination was calculated from the pion lifetime and decay kinematics, and from the beam geometry. The distance from the target in the Bevatron to the bubble chamber was 91 feet. The mean decay length of pions at these energies is 140 to 160 feet. Thus, many of the pions decay in flight. However, the beam is well defined by the various magnets and collimators so that most of the decay muons are lost from it. The maximum decay angle in the laboratory for a muon is about 2.5 deg. One rough calculation divided the beam length into 9 regions and considered what happened to the muons from the beam pions which decayed in each interval. The optics of the beam was taken approximately into account. All pions which decayed in one interval were considered to have come from the center of that interval. A muon which came off at an angle less than that defined by the next collimating aperture was kept. Muons were assumed to be isotropic in the pion c.m.s. The sum of all muons kept from each of the sections were compared with the number of pions left at the chamber. About 12% contamination was calculated in this manner at all three energies. The energy independence of the result is reasonable, if it is considered that more muons fall within a given laboratory angle at higher energies, to compensate for a lower decay rate.

A more detailed calculation was made at one energy, taking the focusing properties of the quadrupoles more strictly into account. Also, all pions before the first quadrupole were considered. A pion unable itself to pass through Q_1 could give rise to a muon which could. Muons kept before the H-magnet were required to be within 1.5% of the mean beam momentum. It was assumed, for lack of more detailed information, that $\frac{d^2\sigma}{dpd\Omega}$ for the pions at the target was a constant for the intervals under consideration. Ray-tracing through the length of the beam showed that a muon had to be within ± 1/4-degree of the axis to pass all the way down the beam channel. Only about 0.4% of the muons from beam pions fitted this criterion. Considerations of pions near the beam momentum led to an estimate that about four times this number of muons would come from pions which would not themselves have reached the aperture of the first quadrupole. Since pions of a higher energy can also give muons of the proper angle and momentum spread (backward decays in the c.m.s.), this number of muons was doubled. The angular definition between Q_1 and the H-magnet is also about ± 1/4-degree. Since only beam pions were present, the number of muons from this region was small. The next region considered was from the H-magnet to the collimator. Again, pions which themselves would not pass through the collimator can give rise to muons which would. About three times as many muons pass through the collimator at small enough angles to reach the chamber, as come from pions which would themselves pass through the collimator. The principal contribution to the muon contamination comes from the region after the collimator. Upper and lower limits on the contamination were found as follows. For the upper limit all muons from decays after the collimator were kept, plus the muons between the H-magnet and the collimator, which remained in the beam, and twice the calculated muons before the H-magnet. The upper limit was 12.8%. The lower limit used the calculated number of muons before the collimator and placed certain restrictions on the muons after the collimator. It amounted to 7.8%. The lower limit was thought to be closer to the actual case. Contamination used was 10.5 ± 3%, where the uncertainty was taken to be somewhat larger than the spread between the two limits

to be conservative. The contamination thus calculated was the percent of muons in the beam just outside the outer wall of the chamber. Some of the pions in the beam would be removed by interactions on passing through the thick part of the pressure vessel. The contamination became 11.7%, 11.2%, and 11.2% at 610, 655, and 750 Mev, respectively. The contamination was slightly higher at 610 Mev, since more of that beam passed through the thick part of the pressure vessel. Otherwise, energy independence was assumed for the contamination, following the results of the simpler calculation.

The electron contamination was measured in the chamber by looking for electrons which radiate more than half of their energy by bremsstrahlung in the propane. Every picture in four rolls at each energy was checked. A mirror was used to look along each track. Curvature templates were used to check whether 50% or more of the energy had been lost. In some cases the entire interaction was recorded: the energy loss and the subsequent conversion of the gamma into a pair. The probability of an electron losing half or more of its energy was found by integrating the expression for the probability of emitting a photon between ν and $\nu + d\nu$.[44] The result of the calculation is that 25% of the electrons will lose the state amount of energy in 50 cm of propane. Electron contaminations found were $2.5 \pm 0.2\%$, $3.8 \pm 0.3\%$, and $2.6 \pm 0.2\%$, at the three energies. Errors were from the statistics of the number of events found.

A check on the track count and contaminations was made by counting all of the interactions of any type in the same pictures in which a track count was made. The mean free path in propane was calculated from the number of tracks and events. Efficiencies for event counting were checked for two rolls. The tracks were corrected for μ and e contaminations as above, and an average effective track length assigned. The measured mean free path was compared with that calculated earlier in this Section, but with the small-angle scatters now removed from the cross section. The agreement was within 7% or better at the three energies. The λ from the measured proton and carbon cross sections had an estimated error between 10% and 15%. The track counting procedure and contaminations were thus well verified.

VI. RESULTS

The number of events found at each energy by the cuts in χ^2 as described in Sec. III were 531, 1159, and 1007. Corrections discussed in Sec. IV and summarized in Table I were applied to the data. The corrected numbers of events were combined with the pion path lengths derived in Sec. V, and the density of hydrogen in propane, to yield total elastic cross sections. The errors from all sources were added together in quadrature to give an over-all error. The resulting errors are about standard deviations. Some errors entering into the over-all error are completely independent from one energy to another, such as the error from statistics. Other errors are almost totally correlated from one energy to another, such as the error on the correction for elastic events outside the cut, because of the identical manner in which they were derived. It would be possible for the cross section at one energy to be too high by a standard deviation, and at another to be too low. However, it is felt more likely for all cross sections to be too high or too low but maintaining the same ratio, since all energies were handled the same. For the remainder of the discussion it will be assumed that the errors are uncorrelated. The total elastic cross sections found were 17.7 ± 2.3 mb, 16.6 ± 1.4 mb, and 14.8 ± 1.4 mb at 610, 655, and 750 Mev, respectively. These cross sections are compared with those determined by other workers in the same energy region in Fig. 10. Erwin and Kopp measured only the branching ratio for elastic scattering and used the total cross section of Cool et al. (Ref. 1) to obtain the elastic values shown at 950 Mev.[20] If the more recent total cross sections of Refs. 12 and 13 are used, then their results should be scaled to the position of the cross shown at that energy. While Baggett measured his own normalization,[17] his total cross section was considerably higher than that of the most recent measurements. Assuming the difference due to incorrect normalization, then it is reasonable to scale his results also. Such a scaling is indicated by the cross at 810 Mev. It is difficult to draw any detailed conclusions from the energy-dependence of the elastic cross section, since the errors on most of the points are large. By keeping within one standard deviation at all of the points, the following

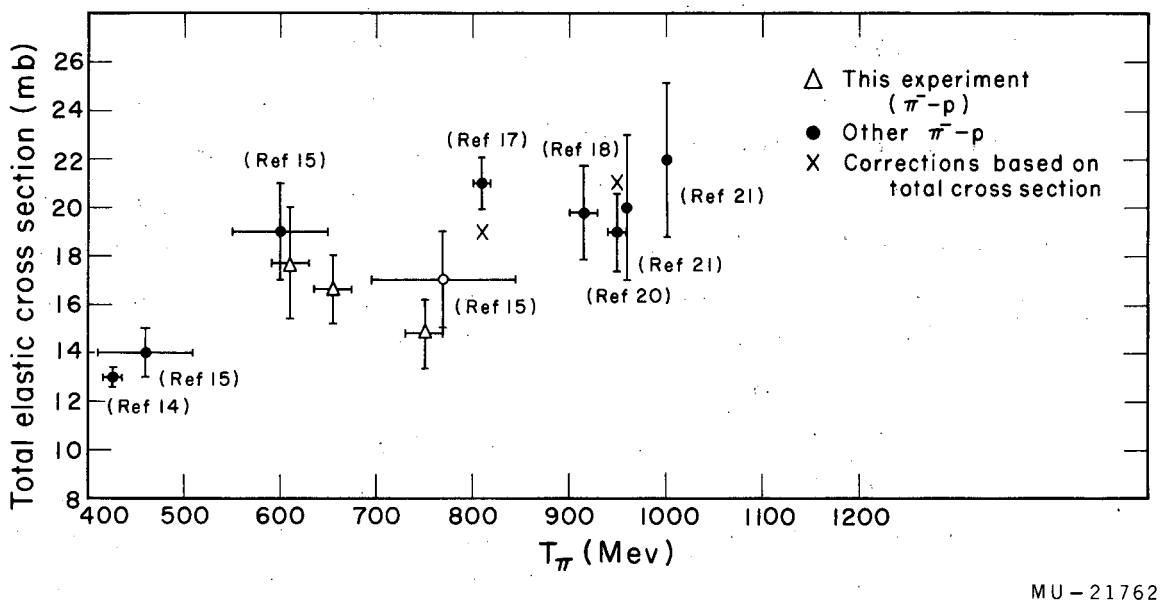

Fig. 10. Total elastic cross section as a function of laboratory kinetic energy. The crosses are possible corrections to the data at those points, as suggested in Sec. VI.

conclusions may be reached. The elastic cross section passes through a maximum near 600 Mev, decreases about 3 mb by 750 Mev, then rises again. No conclusion may be reached as to whether the elastic cross section passes through another maximum around 890 Mev. Indeed, the data indicate that the elastic cross section remains flat in that interval. Above the highest-energy point shown it decreases, reaching 10.1 ± 0.8 mb at 1.44 Bev.[42] The increases around 550 and 800 Mev are quite rapid. A comparison of the mean of the elastic data with the mean of the total cross section data[12, 13] shows that the inelastic cross section rises by about 8 mb from 400 to 600 Mev, and drops approximately 4 to 6 mb to 750 Mev. The magnitude of the inelastic cross section at 600 Mev is about 26 ± 3 mb. The change in the inelastic cross section seems greater and the size is certainly greater than for the elastic cross section, supporting the theory that the peaks are due to inelastic processes.

The normalized differential cross sections are shown in Fig. 11. The number of events in each interval of $\cos \theta^*$ is also shown to indicate the statistical weight of each interval. In addition to the statistical errors, there are normalization and correction errors amounting to $\pm$ 13%, $\pm$ 8.5%, and $\pm$ 9.2% uncertainties at the three energies in the usual order. The forward scattering calculated from the optical theorem and dispersion relations as noted in Sec. IV are shown by the crosses at $\cos \theta^* = 1.0$. The extrapolations to these points are reasonable. The real part of the forward-scattering amplitude, the part given by the dispersion relations, is negligible in comparison to the imaginary part at these energies.[40] This fact, coupled with the large uncertainty in making an independent extrapolation, means that no check of the dispersion relations is possible with these data.

Cosine power-series fits were made to the differential cross sections. The interval $1.0 \geq \cos \theta^* \geq 0.9$ was not used because of the small-angle bias. The next interval is probably not biased. At $\cos \theta^* = 0.9$ the laboratory scattering angle is about 16 deg, and the proton range is about 1.3 cm. It is felt that not many such scatters would be missed. The reasonable extrapolation to the calculated 0 deg value bears

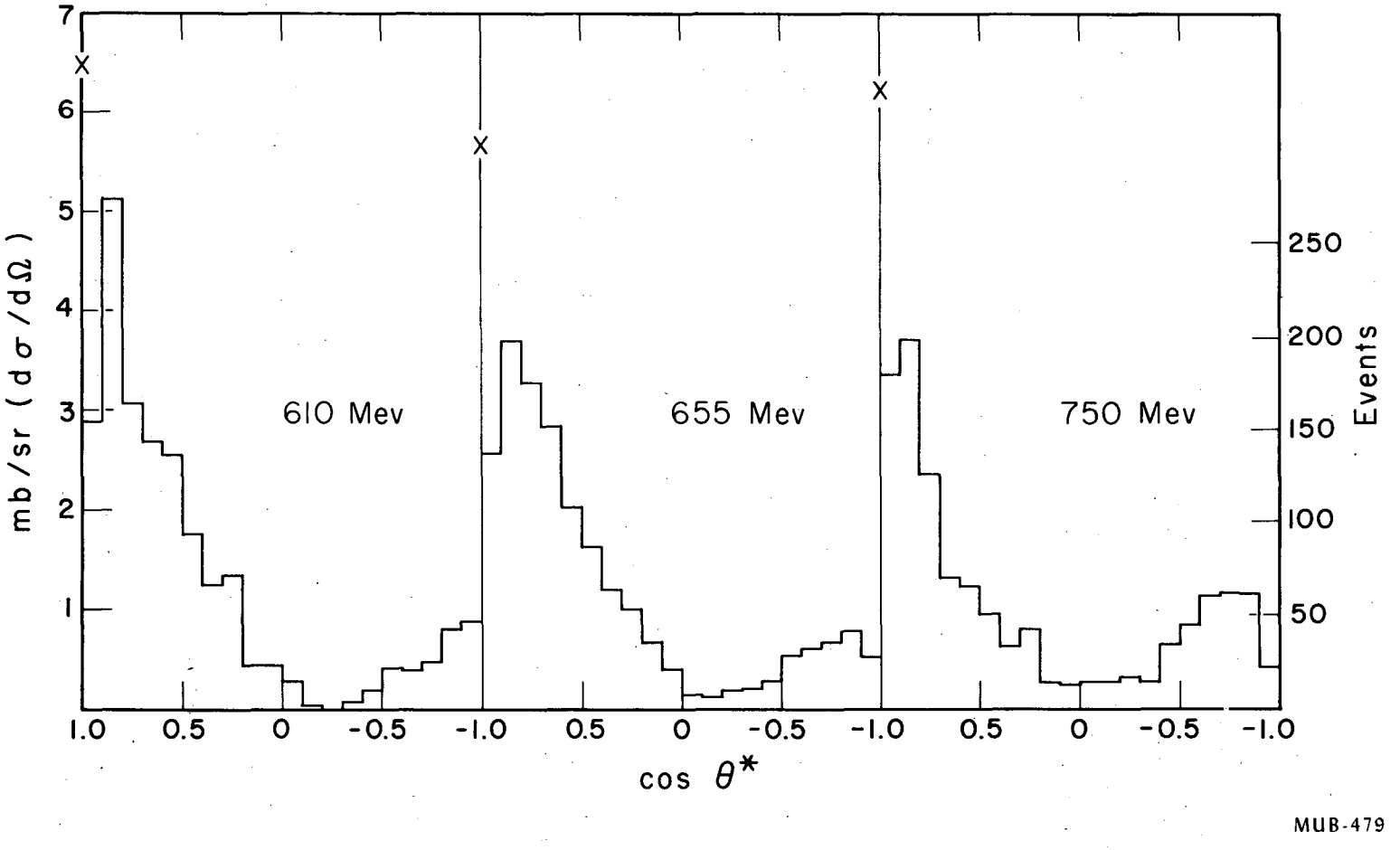

Fig. 11. Differential elastic cross sections at 610, 655, and 750 Mev. The number of events in each interval of cosine is indicated on righthand scale. The forwardmost interval is not corrected for the small-angle bias. Crosses indicate the forward scattering calculated from the optical theorem and dispersion relations (see Sec. VI).

this assumption out. The power series fits were made to the number of events in each interval corrected for the azimuthal bias. The errors used were the square roots of the number of events in each interval, with the errors in the azimuthal correction added in quadrature. All other errors are in the over-all normalization and do not affect the shape of the distribution. The normalization error was put in after the fitting along with the error of fitting. The least-squares program used was IBM 704 PALSI.[45] This program gives the χ^2 of the fit, the coefficients of the terms, the variance-covariance matrix of the coefficients, and calculates the fitted value at each point with the error of the fitted value. The error assigned to the measured value at a given point is supposed to be the "true" error of that point for the proper least-squares fit. Instead, the errors used were those associated with the observed number of counts. To correct for the use of the improper errors, it was assumed that the fitted values at each point were a better representation of the "true" values. The fitting was repeated, using the statistical errors of the fitted number of counts. The coefficients changed little. The fits were made to 19 points ($\Delta \cos \theta^* = 0.10$). As a check, the same data were also divided into 38 points. The same coefficients were again found within the errors.

The variation of χ^2 with the degree of fit was used to select the proper highest power of cosine to be used. The mean value of χ^2 expected from statistical theory is equal to the number of degrees of freedom. The number of degrees of freedom in the case of the 19-point fits was $(18 - n)$, where n is the highest power of cosine in a particular fit. The values of χ^2 were divided by $(18 - n)$ to normalize for the change in the number of degrees of freedom. The results are shown in Fig. 12 for the 19-point iterated fits. The value of $\chi^2/(18 - n)$ reaches a plateau at the proper degree of fit. A fourth-degree fit at 655 Mev and a fifth-degree fit at 750 Mev are clearly indicated. A fourth-degree fit was selected at 610 Mev although a third-degree fit appears almost equally justified. Another criterion for stopping the series is to require the coefficient of the next higher power to be zero within the errors. This criterion selects third, fourth, and fifth degrees. The

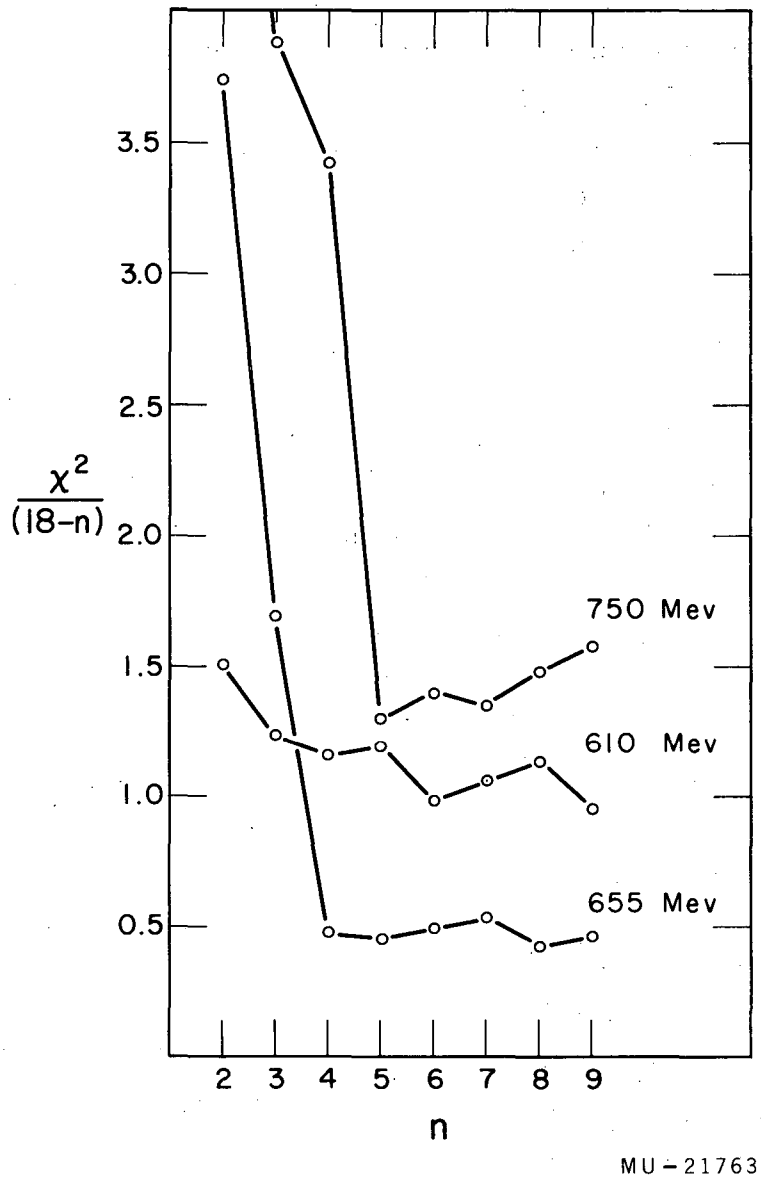

Fig. 12. Variation of χ^2 of the cosine power series fitted to the differential cross sections with degree of the polynomial. Chi-square has been divided by the number of degrees of freedom before plotting.

coefficients of the various powers of cosine of the 19-point iterated fits are given in Table II. The coefficients are in mb/sr and the errors include the normalization errors. The variance-covariance matrices for the best fits are given in Table III. The matrices are symmetric. The off-diagonal terms indicate the degree of correlation between the various coefficients. Normalization errors are not included in Table III. The coefficients are also shown in Figs. 13a-b, along with those of some other workers.[18, 46] The lines connecting the points are to guide the eye from one point to another and do not necessarily represent the proper energy-dependence between the points. Note that Goodwin et al.[14, 46] found it necessary to go to a fifth degree fit around 400 Mev, while it was not necessary to include the fifth power of the cosine until 750 Mev in this work. Bergia et al.[18] found fifth-degree sufficient. The lowest contribution to $(\cos \theta^*)$ comes from D − F wave interference.[5] It seems unlikely that such a term would decrease with increasing energy. So the behavior of a_5 must be attributed to a lack of sensitivity to the higher powers of cosine in this experiment due to the relatively large statistical errors, or to an under-estimation of the errors in the work of Goodwin et al. If a_5 is near zero at 655 Mev, then its increase with energy seems more rapid than might be expected for an interference term between resonant and non-resonant states. So it is perhaps reasonable to assume that the present work was not sensitive to fifth-and higher degrees of cosine. If one goes to fifth order at 610 Mev, the value of a_5 found was 1.52 ± 1.62 mb/sr, which fits with reasonable smoothness with the trend from lower to higher energies.

A complete partial-wave analysis can not be made with the data at hand. Even if isospin formalism, which doubles the number of phase shifts to be found, is ignored, the problem is still under-determined, because the phase shifts are complex. At lower energies the inelastic cross section is small enough so that the imaginary part of a phase shift may be neglected. At these energies the inelastic part is bigger than the elastic part. An analysis through F waves involves the real and imaginary parts of seven phases, while the coefficients of the powers of cosine give only seven numbers. However, the energy variation of the a_n can give some qualitative information.

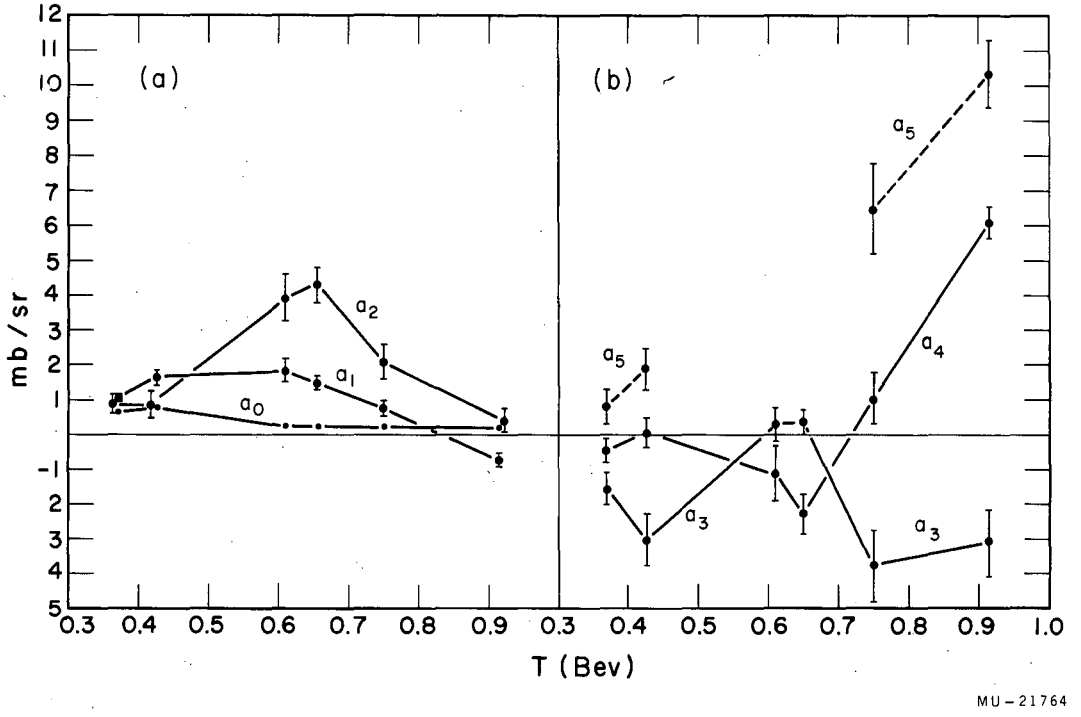

Fig. 13 (a, b). Coefficients of the best fits of $\sum_n a_n(\cos\theta^*)^n$ to the differential cross sections as a function of energy. The straight lines merely connect the various points of a given coefficient together and do not necessarily represent the proper energy dependence between the points. Some of the points of a_2 have been displaced slightly for clarity. See Sec. VI for a discussion of a_5. The points at 370 and 427 Mev are are from Ref. 46, and at 915 Mev from Ref. 18.

TABLE II

Coefficients of the various powers of cosine obtained from least-squares fittings.[a]

Energy (Mev):	370[b]	427[b]	610	655	750	915[c]
a_0	0.66±.03	0.75±.06	0.26±.05	0.26±.04	0.27±.05	0.21±.04
a_1	1.03±.11	1.62±.22	1.83±.32	1.48±.20	0.77±.20	-0.71±.18
a_2	0.89±.25	0.84±.40	3.92±.67	4.31±.50	2.09±.47	0.40±.35
a_3	-1.56±.51	-3.02±.74	0.31±.52	0.37±.35	-3.73±1.06	-3.07±.97
a_4	-0.45±.32	0.05±.44	-1.12±.78	-2.29±.56	1.02±.73	6.10±.44
a_5	0.81±.52	1.91±.63			6.48±1.31	10.35±.95

[a] $\frac{d\sigma}{d\Omega} = \sum_n a_n(\cos\theta^*)^r$, in mb/sr.

[b] These data are from Ref. 46.

[c] Data from Ref. 18.

TABLE III

The variance-covariance matrices of the coefficients of the various powers of cosine.[a]

610 Mev

	0	1	2	3	4
0	.0016	.0047	-.0047	-.0094	.0002
1		.0411	.0443	-.0859	-.1001
2			.1966	-.0813	-.2872
3				.2661	.2805
4					.5814

655 Mev

	0	1	2	3	4
0	.0010	.0014	-.0044	-.0025	.0058
1		.0237	.0257	-.0452	-.0503
2			.1169	-.0495	-.1608
3				.1188	.1286
4					.2779

750 Mev

	0	1	2	3	4	5
0	.0013	.0017	-.0105	-.0111	.0137	.0142
1		.0343	-.0177	-.1567	.0304	.1479
2			.1893	.1882	-.2970	-.2891
3				.9964	-.3496	-1.1005
4					.5352	.5788
5						1.3646

[a]The units are $(mb/sr)^2$. Errors due to normalization, which affect all coefficients at a given energy equally, are not included.

For a qualitative discussion it is more convenient to talk in terms of scattering amplitudes L_J. The scattering amplitudes are related to the phase shifts by

$$L_J = \lambda\!\!\!^{-} \left(\frac{1}{2i}\right)\left(e^{2i\delta_{LJ}} - 1\right) = \left|L_J\right| e^{i\alpha_{LJ}} ,$$

where $\lambda\!\!\!^{-}$ is the c.m.s. wave length divided by 2π. The relation between the magnitude and phase of L_J and the real and imaginary parts of the phase shift, a_{LJ} and b_{LJ}, is given in Fig. 14. Note that the phase of L_J is the same as the real part of the phase shift only when the imaginary part of the phase shift is zero. The elastic cross section for a given L and J is

$$\sigma_{LJ}^{elas} = 2\pi (2J + 1) \left|L_J\right|^2 .$$

The inelastic cross section for a given L and J is

$$\sigma_{LJ}^{inel} = \frac{1}{2} \pi (2J + 1) \lambda\!\!\!^{-2} \left[1 - \exp(-4b_{LJ})\right].$$

The values of $\lambda\!\!\!^{-2}$ at the energies under consideration are 1.89, 1.73, and 1.46 mb.

The expansion of the differential elastic cross section into partial waves with the neglect of isospin is[47]

$$\frac{d\sigma}{d\Omega} = \left|\sum_{\ell} \left[(\ell + 1) L_{\ell + \frac{1}{2}} + \ell L_{\ell - \frac{1}{2}}\right] P_\ell (\cos\theta^*)\right|^2$$

$$+ \left|\sum_{\ell} \left[L_{\ell + \frac{1}{2}} - L_{\ell - \frac{1}{2}}\right] \sin\theta^* \frac{d}{d(\cos\theta^*)} P_\ell (\cos\theta^*)\right|^2$$

in the above notation. The evaluation of this expression through F waves has been carried out in Table IV. All of the contributions to a given power of cosine have been gathered in one column. An interference term labeled symbolically by $L_J L'_{J'}$ means the numerical coefficient of

$$\left|L_J\right| \left|L'_{J'}\right| \cos\left(a_{LJ} - a_{L'J'}\right) .$$

It should be re-emphasized that the phases here are the phases of the amplitudes, not the real parts of the phase shifts.

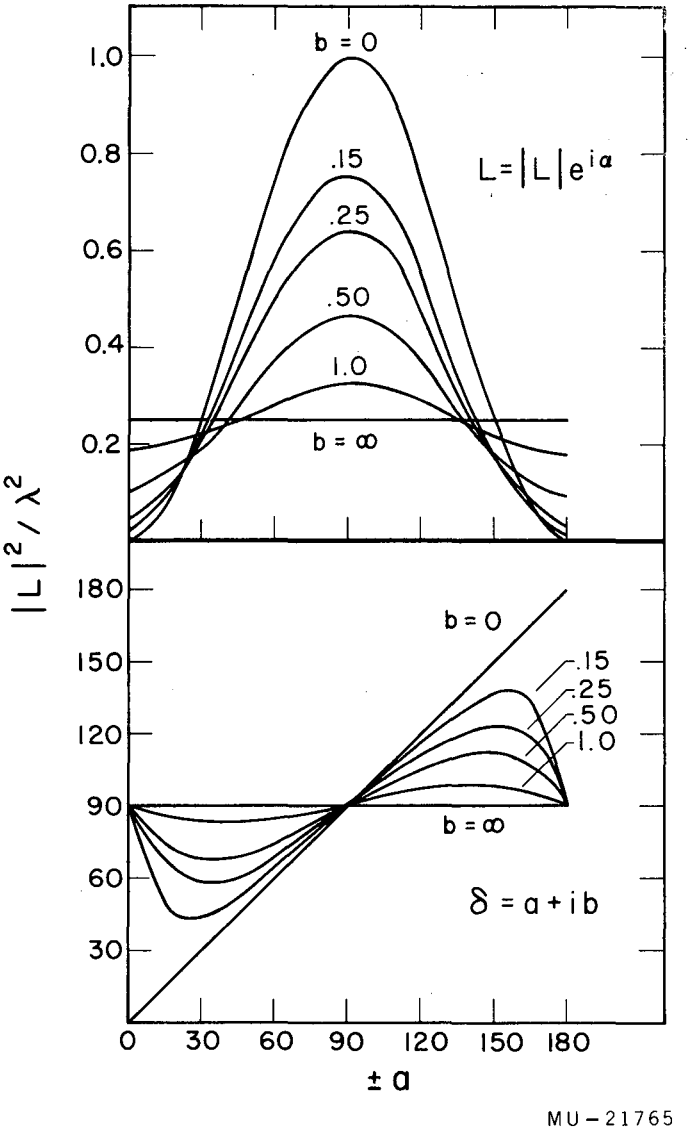

Fig. 14. Variation of the magnitude and phase of the scattering amplitude, as defined in Sec. VI, with the real and imaginary parts of the phase shift, where $L = |L| e^{ia}$, and $\delta = a + ib$.

TABLE IV

Contributions of the partial wave amplitudes to the various powers of cosine.[a]

	a_0	a_1	a_2	a_3	a_4	a_5	a_6
$S_{1/2}P_{1/2}$		2					
$S_{1/2}P_{3/2}$		4					
$S_{1/2}D_{3/2}$	-2		6				
$S_{1/2}D_{5/2}$	-3		9				
$S_{1/2}F_{5/2}$		-9		15			
$S_{1/2}F_{7/2}$		-12		20			
$P_{1/2}P_{3/2}$	-2		6				
$P_{1/2}D_{3/2}$		4		0			
$P_{1/2}D_{5/2}$		-9		15			
$P_{1/2}F_{5/2}$	-3		9		0		
$P_{1/2}F_{7/2}$	3		-30		35		
$P_{3/2}D_{3/2}$		-10		18			
$P_{3/2}D_{5/2}$		0		12			
$P_{3/2}F_{5/2}$	3		-36		45		
$P_{3/2}F_{7/2}$	-3		-6		25		
$D_{3/2}D_{5/2}$	3		-36		45		
$D_{3/2}F_{5/2}$		0		12		0	
$D_{3/2}F_{7/2}$		21		-110		105	
$D_{5/2}F_{5/2}$		$\frac{45}{2}$		-117		$\frac{225}{2}$	
$D_{5/2}F_{7/2}$		9		-30		45	
$F_{5/2}F_{7/2}$	$-\frac{9}{2}$		$\frac{207}{2}$		$-\frac{675}{2}$		$\frac{525}{2}$

TABLE IV (Continued)

	a_0	a_1	a_2	a_3	a_4	a_5	a_6
$\lvert S_{1/2}\rvert^2$	1						
$\lvert P_{1/2}\rvert^2$	1						
$\lvert P_{3/2}\rvert^2$	1		3				
$\lvert D_{3/2}\rvert^2$	1		3				
$\lvert D_{5/2}\rvert^2$	$\frac{9}{4}$		$-\frac{9}{2}$		$\frac{45}{4}$		
$\lvert F_{5/2}\rvert^2$	$\frac{9}{4}$		$-\frac{9}{2}$		$\frac{45}{4}$		
$\lvert F_{7/2}\rvert^2$	$\frac{9}{7}$		$\frac{45}{4}$		$-\frac{165}{4}$		$\frac{175}{4}$

[a]Read down a column for all of the contributions to a given a_n. An interference term indicated symbolically by $L_J L'_{J'}$ means the contribution of $\left|L_J\right| \left|L'_{J'}\right| \cos(a_{LJ} - a_{L'J'})$.

It will be assumed that the coefficient a_2 actually reaches a maximum at 600 Mev, instead of at 650 Mev as indicated in Fig. 13a. It will also be assumed that the peak at 600 Mev is due to a single state passing through a maximum, whether a resonance is involved or not. The positive peak in a_2 then indicates a $J = 3/2$ wave has a maximum at 600 Mev. $J = 5/2$ waves have a negative a_2. $J = 7/2$ is ruled out because a_4 and a_6 should be about four times as large as a_2. The increase of a_4 and decrease of a_2 are consistent with a $J = 5/2$ wave becoming important. It is not known at present if a_4 passes through a maximum around 890 Mev. While it seems probable that a $J = 3/2$ amplitude has a maximum near 600 Mev, it resonance or non-resonance is not established. For an amplitude to have a non-resonant maximum, the real and imaginary parts of the phase shift must increase and n must decrease, since both the elastic and inelastic cross sections have maxima. The changes observed are rapid. There is a general theorem which limits how rapidly a phase shift may decrease.[48] The observed rapid change probably requires that the phase shift be increasing through +90°, if the peak is to be ascribed to a single wave. It will be assumed that the amplitudes really exhibit resonant behavior for most of what follows. If $J = 3/2$ and $J = 5/2$ are concluded for the two resonances, then the increase of a_5 and decrease of a_3 are the result of the increasing $J = 5/2$ wave interfering with a non-resonant $J = 5/2$ or $7/2$ wave. Little can be said about a_0 and a_1 because so many terms contribute to them.

The L values of the two peaks can not be established uniquely from just these data. The relative parities of the two states can be tentatively established. If the states have even relative parity, the interference term is proportional to $(3 - 36\cos^2\theta^* + 45\cos^4\theta^*)$. For odd relative parity the interference term is $12\cos^3\theta^*$. In the foregoing it has been assumed that the cosine of the difference in phases is positive. If one of the resonant waves has positive phase and the other negative, then the cosine is negative for any reasonable assumptions about the real and imaginary parts of the phase shift. However, it is unlikely that one phase is negative from general considerations and from the data (see below). Since both peaks are strongly inelastic it is unlikely that the

difference in the phases of the amplitudes ever approaches 90 deg in the energy range 600 to 900 Mev (see Fig. 14). So the interference terms should be present and reasonably important and have the signs indicated above. For the widths and spacing of the peaks it is reasonable to assume that the interference term is roughly constant in the energy range just mentioned. In particular, if the interference term is important at around 650 Mev, then even relative parity is ruled out by the large positive value of a_2 and the large negative value of a_4. Unfortunately, the possible contribution of the even-parity interference term around 750 to 900 Mev is masked by that of the $J = 5/2$ waves in absolute square. If one of the resonant waves has positive phase while the other has negative phase, then the even-parity interference term should give approximately constant positive contributions to a_2 and negative to a_4. Such contributions would make the observed energy dependence of those coefficients harder to explain. Odd relative parity, on the other hand, seems compatible with the observed coefficients. There must be large contributions to a_3 from the interference of many non-resonant states. Indeed it has already been noted that the large increase of a_5 requires a non-resonant state. The same interference terms give a large negative contribution to a_3. Thus it is more reasonable to assign odd relative parity to the two resonances. In other words, the two resonances are either $P_{3/2}$ and $D_{5/2}$, or $D_{3/2}$ and $F_{5/2}$.

The negative value of a_4 around 650 Mev must still be explained by introducing some non-resonating states with phases to give a negative cosine of the phase difference. There is ample freedom to introduce the necessary states.

If the real part of the phase shift is near 90 deg for the $J = 3/2$ wave at 600 Mev, then that wave must be strongly absorbed to account for the observed elastic to inelastic ratio. (As an aside it may be pointed out that the concept of the real part of a phase shift is no longer defined for a completely absorbed wave.) The inelastic cross section is 26 ± 3 mb at 600 Mev. Near 90 deg for the real part of the phase shift the elastic scattering is always greater than or equal to the inelastic. Equality comes only with full absorption of the wave (cf. Fig. 14).

A fully absorbed J = 3/2 wave can give only 11.9 mb of inelastic scattering, and contributes another 11.9 mb to the elastic scattering at 610 Mev. All of the other non-resonant waves must contribute the remaining 6 mb of elastic and 14 mb of inelastic scattering. It would be difficult to obtain the proper amount of inelastic scattering if the resonant J = 3/2 wave were absorbed less. In the latter case there would be more inelastic and less elastic scattering to be fit by the non-resonant waves. This task would be difficult since it is impossible to have inelastic scattering without any elastic scattering. Strong absorption of the resonant wave is predicted by Peierls' conjecture.[24]

If the peak at 600 Mev is not a true resonance, then the conclusions of the previous paragraph need no longer hold. The elastic to inelastic ratio is then easier to obtain. But the difficulty of explaining the rapid change in cross section, particularly the decrease, remains. The scattering amplitudes of several waves would have to increase and then decrease, all at roughly the same energy, to account for the change in the elastic and inelastic cross sections. Interference terms vanish in the total elastic and inelastic cross sections, so they may not be invoked. While such "cooperation" of several partial waves can not be ruled out, it seems unlikely.

It is possible to construct reasonable sets of non-resonating waves which, with the above resonant waves, can fit the observed coefficients of the cosine power series. The solution is not unique, since the problem is under-determined as already noted. No significance is attached to these sets because of the lack of uniqueness. They are mentioned merely to show that a consistent set of scattering amplitudes could be constructed with the assumption of $P_{3/2}$ and $D_{5/2}$, or $D_{3/2}$ and $F_{5/2}$ for the resonances.

A phase shift analysis has been attempted up to 600 Mev by Walker, Davis and Shephard.[49] They used charge exchange and π^+ – proton scattering data, and assumed fixed values for some of the imaginary parts of the phase shifts. They also required a smooth variation of the phase shifts with energy. They found a $D_{3/2}$ phase shift at 600 Mev of $18.3 \text{ deg} \begin{smallmatrix} +35 \text{ deg} \\ -0 \text{ deg} \end{smallmatrix} + i \left(0.65 \begin{smallmatrix} +0.49 \\ -0.32 \end{smallmatrix}\right)$. This phase was the only one

approaching 90 deg. Attempts to start the computer search program with the $D_{3/2}$ phase at 90 deg ended with no satisfactory fits.[50] However, the problem was under-determined for them also, and they used some poorly determined data. It is felt that their results are not conclusive. However, their enhanced J = 3/2 wave agrees with the results of this experiment.

Moravisck[51] has suggested that the polarization of the recoil protons from π^--proton scattering at and near 90 deg (pion c.m.s. angle) be measured to resolve the ambiguities in the assignments. Unfortunately the differential cross section at that angle is very small at these energies (see Figs 11a-c), so the experiment would be very difficult to perform.

VII ACKNOWLEDGMENTS

The support of Dr. Wilson Powell is gratefully acknowledged. Dr. Oreste Piccioni, Dr. William Fowler, and Dr. Robert Birge helped immensely with the early stages of this experiment. We would like to thank Dr. Edward Lofgren and the Bevatron crew for their help and skill in beam sharing, and Larry Oswald and the bubble chamber crew for chamber operations. Jack Hohenstein did much of the scanning and has been indispensable in helping to compile the data. Edith Goodwin and Herbert Holden also helped with the scanning. Howard White and his staff are thanked for the data reduction. All of the measures who measured the more than 20 000 origins necessary for this experiment are thanked. The author has consulted frequently with Peter Newcomb.

This work was done under the auspices of the U. S. Atomic Energy Commission.

REFERENCES

1. R. Cool, O. Piccioni, and D. Clark, Phys. Rev. 103, 1082 (1956).
2. M. Heinberg, et al., Phys. Rev. 110, 1211 (1958).
3. F. P. Dixon and R. L. Walker, Phys. Rev. Letters 1, 142 (1958).
4. F. P. Dixon and R. L. Walker, Phys. Rev. Letters 1, 458 (1958).
5. P. C. Stein and K. C. Rogers, Phys. Rev. 110, 1209 (1958).
6. J. W. DeWire, H. E. Jackson, and Raphael Littauer, Phys. Rev. 110, 1208 (1958).
7. J. I. Vette, Phys. Rev. 111, 622 (1958).
8. H. H. Bingham and A. B. Clegg, Phys. Rev. 112, 2053 (1958).
9. K. Berkelman and J. A. Waggoner, Phys. Rev. 117, 1364 (1960).
10. Robert R. Wilson, Phys. Rev. 110, 1212 (1958).
11. H. C. Burrowes et al., Phys. Rev. Letters 2, 119 (1959).
12. T. J. Devlin et al., Phys. Rev. Letters 4, 242 (1960).
13. J. C. Brisson et al., Phys. Rev. Letters, 3, 561 (1959).
14. L. K. Goodwin, R. W. Kenney, and V. Perez-Mendez, Phys. Rev. Letters 3, 522 (1959).
15. R. R. Crittenden et al., Phys. Rev. Letters 2, 121 (1959).
16. Neyer, Levêque, Lehmann, Revel, and Gaillard . Private communication.
17. Lee Baggett, Jr., π^--p Elastic Scattering and Single Pion Production at 0.939 Bev/c (M. S. Thesis), UCRL-8302, May 1958 (Unpublished).
18. S. Bergia et al., Nuovo cimento 15, 551 (1960).
19. B. T. Feld, B. Maglić, and C. A. Diffey, Bull. Am. Phys. Soc. II 4, 447 (1959).
20. A. R. Erwin Jr. and J. K. Kopp, Phys. Rev. 109, 1364 (1958).
21. W. D. Walker, F. Hushfar, and W. D. Shephard, Phys. Rev. 104, 526 (1956).
22. I. Derado and N. Schmitz, Phys. Rev. 118, 309 (1960).
23. Ronald F. Peierls, Phys. Rev. Letters 1, 174 (1958).
24. Ronald F. Peierls, Phys. Rev. 118, 325 (1960).
25. L. F. Landovitz and L. Marshall, Phys. Rev. Letters 3, 190 (1959).
26. Michael J. Moravcsik, Phys. Rev. 104, 1451 (1956).

27. A. M. Wetherell, Phys. Rev. 115, 1722 (1959).
28. P. C. Stein, Phys. Rev. Letters 2, 473 (1959).
29. J. J. Sakurai, Phys. Rev. Letters 1, 258 (1958).
30. G. B. Chadwick et al., Phys. Rev. Letters 4, 611 (1960).
31. Wen-Nong Wong and Marc Ross, Phys. Rev. Letters 3, 398 (1959).
32. Peter Carruthers, Phys. Rev. Letters 4, 303 (1960).
33. P. Carruthers and H. A. Bethe, Phys. Rev. Letters 4, 536 (1960).
34. W. M. Powell, W. B. Fowler, and L. O. Oswald, Rev. Sci. Instr. 29, 874 (1958).
35. Frank Solmitz, LRL Eng. Note 4320-60 M6, Nov. 21, 1957 (unpublished).
36. Richard G. Thomas, Jr. UCRL-8965 (Thesis) (unpublished).
37. H. Bethe, Phys. Rev. 70, 821 (1946).
38. W. T. Scott, Phys. Rev. 76, 212 (1949).
39. G. Molière, Z. Naturforsch. 3a, 78 (1948). See also E. Segrè, editor, Experimental Nuclear Physics, Vol. 1 (John Wiley and Sons, New York, 1953) pp. 287-290.
40. James W. Cronin, Phys. Rev. 118, 824 (1960).
41. L. O. Roellig and D. A. Glaser, Phys. Rev. 116, 1001 (1959).
42. M. Chrétien, et al., Phys. Rev. 108, 383 (1957).
43. J. W. Cronin, R. Cool, and A. Abashian, Phys. Rev. 107, 1121 (1957).
44. E. Segrè, editor, Experimental Nuclear Physics, Vol. 1 (John Wiley and Sons, New York, 1953) p. 260.
45. Richard E. von Holdt, UCRL-5504 (PALSI--A Polynomial Approximating Code. March 10, 1959), unpublished.
46. Lester K. Goodwin, UCRL-9119 (Thesis) (unpublished). Also private communication to obtain the fifth-order fits at 427 Mev. The errors on these points were obtained by this author from the errors on the Legendre polynomial fits from UCRL-9119 .
47. E. M. Henley, M. A. Ruderman, and J. Steinberger, Annual Review of Nuclear Science, Vol. 3 (Annual Reviews, Inc. 1953).
48. Steven Weinberg. (Lawrence Radiation Laboratory) Private communication.

49. W. D. Walker, J. Davis, and W. D. Shephard, Phys. Rev. 118, 1612 (1960).

50. John H. Scandrett. (University of Wisconsin) Private communication.

51. Michael J. Moravcsik, Phys. Rev. 118, 1615 (1960).